Catalysis Today 427 (2024) 114414

Contents lists available at ScienceDirect

Catalysis Today

journal homepage: www.elsevier.com/locate/cattod

Catalytic activity of Ni-$MgAl_2O_4$ modified with transition metal (Ti, Mo, W) carbides as potential catalysts for resource recovery via dry reforming of waste plastics

Ewelina Pawelczyk [a,*], Izabela Wysocka [a,*], Tomasz Dymerski [b], Jacek Gębicki [a]

[a] Department of Process Engineering and Chemical Technology, Faculty of Chemistry, Gdansk University of Technology, Narutowicza 11/12 St., 80-233 Gdansk, Poland
[b] Department of Analytical Chemistry, Faculty of Chemistry, Gdansk University of Technology, Narutowicza 11/12 St., 80-233 Gdansk, Poland

ARTICLE INFO

Keywords:
Carbide
Catalysts
Waste management
Hydrogen
Sustainable production
Co2

ABSTRACT

The growing amounts of plastic waste and CO_2 emissions are two environmental threats that require urgent attention. Pyrolysis combined with dry reforming (PCDR) is a technology that allows both CO_2 utilization and resource recovery from waste plastic. New catalysts for PCDR are crucial for developing efficient and stable processes that can be widely implemented in the industry. In this study, Ni/$MgAl_2O_4$ catalysts modified using different transition metal (Ti, Mo, W) carbides were investigated in the PCDR of low-density polyethylene (LDPE) and polystyrene (PS) with emphasis on syngas yield, H_2/CO ratio, product distribution, and catalyst deactivation. In addition, the effect of reforming temperature and process pressure was investigated. The catalysts were characterized using H_2-TPR, CO_2-TPD, N_2 physisorption, XRD, TEM, XPS and TGA. The combined characterization and activity tests demonstrated that modification with different metal carbides affects the structure and activity of Ni/$MgAl_2O_4$ catalysts in relation to product yields, syngas composition, and catalyst stability. The investigation revealed that modification of nickel catalysts with different transition metal carbides enables manipulation of syngas composition, which is of great importance because different industrial processes require synthesis gas with different H_2:CO ratios. Moreover, mixed outcomes were observed when different plastic feedstocks were used in the PCDR, indicating that different metal carbide-modified catalysts may be suitable for the process depending on the feedstock used. Regarding the effectiveness of synthesis gas production and catalyst stability, the most promising catalyst was the Ni-TiC/$MgAl_2O_4$ catalyst. According to the obtained results, modification with TiC resulted not only in increased synthesis gas production but also in reduced carbon deposition in PCDR of both LDPE and PS.

1. Introduction

Climate change and the growing amount of contaminants in the environment are threats of global importance that require urgent management. The European Union target linked to the circular economy is to achieve municipal waste recycling of 55% and 65% by 2025 and 2035, respectively. What is more, the maximum limit for plastic waste storage in landfills cannot exceed 10% by 2035. In 2020, the high demand for plastic materials led to a global production of 367 Mt [1]. During the past 60 years, only 9% of the plastic waste produced has been recycled [2]. This clearly indicates the need for other waste-management methods. Currently implemented treatment techniques include landfill and incineration. While landfilling waste plastics has no economic benefits, waste incineration allows the recovery of raw materials in the form of thermal energy. However, both methods result in the release of harmful substances into soil, groundwater, and air [3,4]. As specified by the European Union's sustainable development policy, landfilling and incineration of waste must be reduced and step by step replaced by other, more environmentally friendly methods of waste management [5]. Another emerging environmental issue is the constantly increasing emissions of greenhouse gases (GHGs), which contribute to climate change [6–8]. Among them, carbon dioxide, owing to its leading content in the atmosphere, is characterized by the largest contribution to the greenhouse effect. Therefore, carbon capture and utilization technologies have received significant attention. The development of a pro-environmental technology that combines plastic waste processing

* Corresponding authors.
E-mail addresses: ewelina.pawelczyk@pg.edu.pl (E. Pawelczyk), izabela.wysocka@pg.edu.pl (I. Wysocka).

https://doi.org/10.1016/j.cattod.2023.114414
Received 14 February 2023; Received in revised form 18 August 2023; Accepted 11 October 2023
Available online 14 October 2023
0920-5861/© 2023 The Author(s). Published by Elsevier B.V. This is an open access article under the CC BY-NC-ND license (http://creativecommons.org/licenses/by-nc-nd/4.0/).

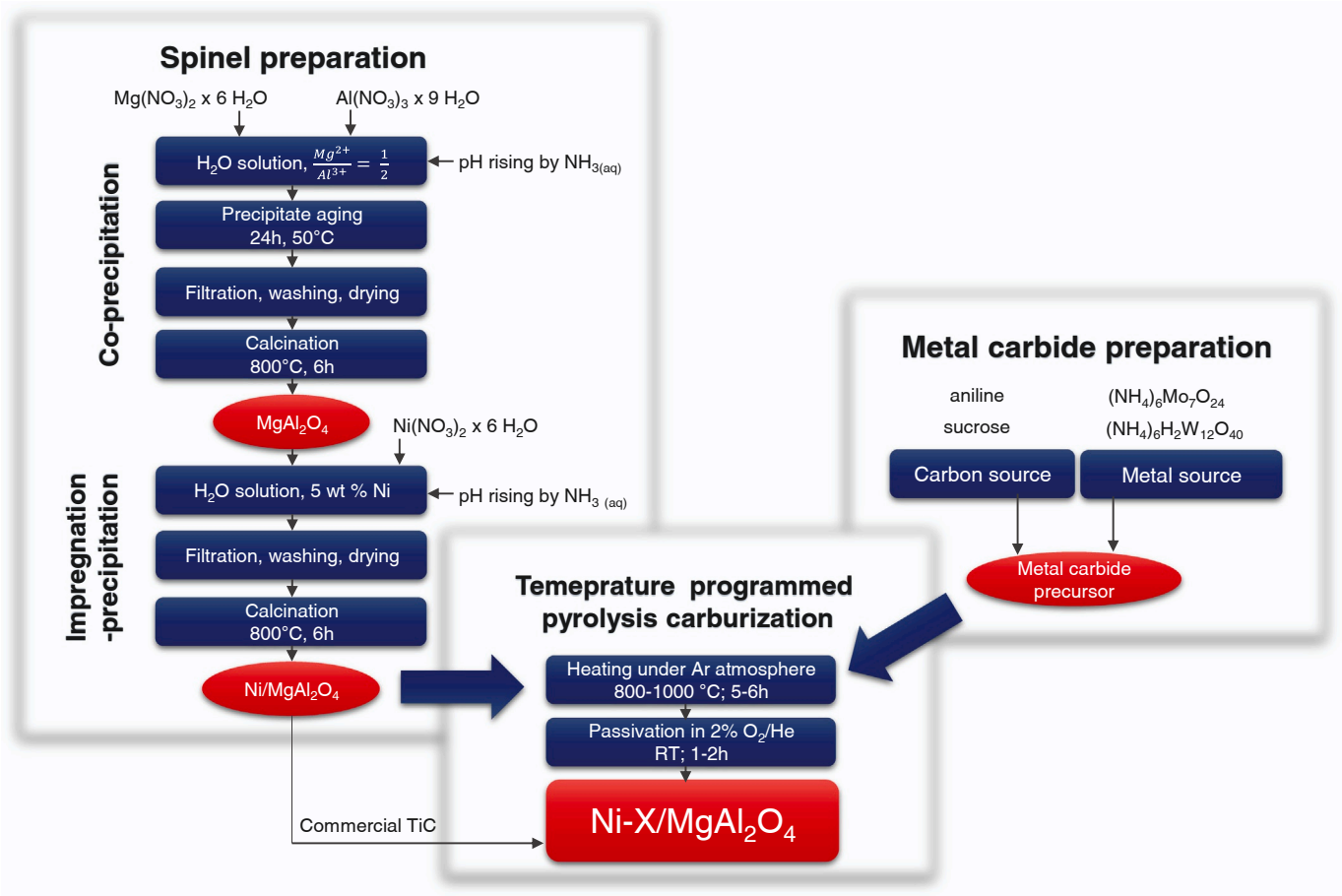

Fig. 1. Simplified scheme of catalysts' preparation.

and CO_2 utilization is fundamental for a circular economy and sustainable development.

The pyrolysis-catalytic-dry reforming (PCDR) process holds great potential for utilization of both carbon dioxide and residual plastic materials. This technology allows for resource recovery and valorization of plastic waste - hydrocarbon carriers, which may serve as suitable feedstock for generating valuable outputs like hydrogen and syngas, which find extensive application across different industries. [9–11]. PCDR involves two stages: pyrolysis of plastic feedstock and subsequent dry reforming of obtained hydrocarbons. The dry reforming of hydrocarbons can be expressed by overall Eq. 1. It is highly endothermic process, for instance, depending on the hydrocarbon feedstock, ΔH is equal to 428.1 kJ/mol [12], 817.1 kJ/mol [12] and 644.8 kJ/mol [13] for ethane, butane and propane, respectively. Therefore, suitable catalysts are crucial to reduce required thermal energy. So far, there are only a few reports in the literature regarding tests of catalysts in PCDR processes, and they are mainly based on nickel or cobalt, owing to their reduced expense relative to noble metals. However, currently used catalysts suffer from deactivation and are not sufficiently effective, which prevents such technology from being accepted and widely applied for waste plastics [9,14,15].

$$C_xH_y + xCO_2 = 2xCO + y/2\ H_2\ \Delta H > 0 \quad (1)$$

Transition metal carbides (TMCs) have gained attention as catalysts for many catalytic processes, such as CO oxidation, hydrogenation, and dry reforming (DR) of hydrocarbons, as they exhibit advantageous characteristics like elevated catalytic activity, thermal stability, and the ability to withstand the presence of impurities such as sulfur and chlorides within the reaction environment. [16–19]. Moreover, their catalytic activity has been reported in dry reforming, not limited to methane, but extending to other hydrocarbons as well., which makes them suitable candidates for the reforming of hydrocarbons generated in the pyrolysis step of PCDR [13,20–22]. Furthermore, in the dry reforming reaction, TMCs posess extraordinary potential to reduce the formation of carbon deposits due to the unique oxidation-recarburization cycles they undergo under DR conditions. In the oxidation step, CO_2 is reduced to carbon monoxide. Subsequently, during the recarburization step, carbon atoms derived in hydrocarbon cracking and CO disproportionation are built into the structure of carbide, which hinders catalyst deactivation by forming carbon deposits on the surface of the catalyst [16,18,19]. Moreover, in the literature, there are reports indicating the beneficial effects of modifying TMC catalysts with nickel on the dry reforming process, such as promoting structural stability and decreasing Ni particle size, hence improving catalytic performance [23–28]. Additionally, the addition of other metals to the carbide catalyst may increase the H_2/CO ratio of the syngas generated in the DR. Therefore, the integration of a carbide catalyst alongside a conventional metal oxide-based nickel catalyst presents a viable approach, enabling the creation of an efficient and stable process for the production of high-quality synthesis gas.

Therefore, this study presents the first approach to the use of catalysts modified with transition metal carbides in the process of pyrolysis combined with the dry reforming (PCDR) of plastic waste. Catalysts $NiMgAl_2O_4$, Ni-TiC/$MgAl_2O_4$, Ni-Mo_2C/$MgAl_2O_4$ and Ni-WC/$MgAl_2O_4$ were investigated to determine the effect of the modification with metal carbides in relation to syngas yield, H_2:CO molar ratio, catalyst deactivation as well as product distribution. The impact of plastic feedstock was investigated using two polymers representing different types of plastic waste in the environment: low-density polyethylene (LDPE) and polystyrene (PS). In addition, the effect of reforming temperature and process pressure was investigated.

MOST WIEDZY Downloaded from mostwiedzy.pl

2. Materials and methods

2.1. General procedure for synthesis of catalysts

Magnesia-alumina spinel was synthesized through chemical precipitation in an alkaline medium. Magnesium nitrate and aluminum (III) nitrate were dissolved in deionized water to achieve an Mg^{2+}:Al^{3+} molar ratio of 0.5. The solution's pH was adjusted to 10 using a 25% aqueous ammonia solution while constantly stirring. The resultant $MgAl_2O_4$ precipitate was then aged at 50 °C for 24 h. After this time, the precipitate was separated, washed twice with deionized water, and subsequently dried at 80 °C. The last step involved calcination for 6 h at 800 °C. The Ni/$MgAl_2O_4$ catalyst was synthesized through impregnation and precipitation on a previously obtained magnesia-alumina spinel support. The $MgAl_2O_4$ support was suspended within a solution of nickel nitrate, and the suspension's pH was subsequently modified to 9 to facilitate the precipitation of nickel particles. The resulting Ni/$MgAl_2O_4$ was then isolated, subjected to two rounds of washing with deionized water, dried at a temperature of 80 °C, and ultimately calcined at 800 °C for a duration of 6 h.

Catalysts modified with Mo_2C and WC were prepared using temperature programmed pyrolysis-carburization of organic-inorganic precursors, while TiC-modified catalyst was obtained by impregnation-precipitation method using commercially available TiC (Sigma-Aldrich). The reagents were added in such an amount that the nickel particles were 5 wt%, whereas the support:carbide mass ratio was 2:1. A simplified diagram of the catalyst synthesis is shown in Fig. 1.

Ni-TiC/$MgAl_2O_4$ catalyst was prepared using wet impregnation and precipitation method. Previously obtained $MgAl_2O_4$ spinel support and commercial TiC (Sigma Aldrich) were suspended in nickel nitrate solution. The suspension's pH was adjusted to 9 to induce the precipitation of nickel particles. Subsequently, the resulting Ni-TiC/$MgAl_2O_4$ was separated, subjected to two rounds of washing using deionized water, and dried under vacuum conditions at a temperature of 50 °C for 24 h. Afterwards, dried powder was calcined at 800 °C for 6 h under inert gas atmosphere.

The first step in the preparation of the Ni-Mo_2C/$MgAl_2O_4$ catalyst involved the preparation of an organic-inorganic molybdenum-amine precursor. The ammonium heptamolybdate was dispersed in deionized water. Then, aniline was added in a four-fold excess over molybdenum ions. The solution's pH was adjusted to 4 by using 1 M HCl until a precipitate was formed. The suspension of the MoOx-amine precursor was aged at 50 °C for 4 h. After aging, the solid was separated, washed with deionized water, and dried at 50 °C for 24 h. The next step involved the dispersion of the previously prepared Ni- $MgAl_2O_4$ in water with a MoOx-amine precursor and stirring for 2 h. The solid was then separated, dried, and ground in an agate mortar and pestle. The final step involved annealing the obtained solid in a tubular reactor under a continuous flow of argon. The temperature increase was maintained at 10 °C/min until it reached 800 °C. The temperature of 800 °C was maintained for 5 h, and then the reactor was cooled to room temperature in an inert atmosphere. After the reactor reached room temperature, the composite obtained was passivated in a stream of 2% O_2 in He for 2 h.

Similarly, the Ni-WC/$MgAl_2O_4$ catalyst was synthesized in two steps: the preparation of organic-inorganic precursors (W-Ni-saccharide) and thermal treatment in an inert atmosphere. In the first step, solid ammonium metatungstate (AMT), nickel nitrate hexahydrate, and the $MgAl_2O_4$ spinel support were added to an aqueous sucrose solution, which was then transferred to a stainless-steel reactor with a Teflon vessel and subjected to hydrothermal treatment at 180 °C for 24 h. The resulting precursor mixture was withdrawn from the reactor dried under vacuum at 80 °C. In the next step, the dried powder was placed in a stainless-steel tube and heated in a tube furnace at 980 °C (heating rate 10 °C/min) for 6 h under an argon atmosphere. After cooling to room temperature in an argon atmosphere, passivation was performed using a 2% O_2/He mixture (50 ml/min) for 1 h.

2.2. Catalyst characterization

The reducibility and active phase-support interactions were examined using H_2-TPR analysis. The analysis was carried out in the temperature range of 100–900 °C with a heating rate of 10 °C/min under 10% H_2 in Ar (100 ml/min). Prior to the analysis, the catalyst sample (100 mg) was pre-treated under helium stream (100 ml/min) for 1 h at 100 °C.

The basicity of catalysts was determined using CO_2-TPD analysis. The previously reduced catalyst was saturated under 20% CO_2/He flow at 50 °C for 1 h. Then, the catalyst sample was purged with He stream at 50 °C for 1 h. The CO_2-TPD analysis was carried out at the temperature range from 50 °C to 900 °C with a ramp of 10 ∘C/min under He stream. The desorbed CO_2 was detected using thermal conductivity detector (TCD) andt desorbed CO_2 amount was obtained by integrating the TPD profile.

Nitrogen adsorption isotherms, pore size distributions and total pore volumes were determined using surface area analyser Micrometrics Gemini V at − 196 °C. Before conducting the measurements, catalyst sample underwent a vacuum degassing process at 200 °C for 2 h. Nitrogen adsorption isotherms were determined within the p/p_0 range from 0.05 to 0.99. Specific surface areas were calculated on the basis of Brunauer-Emmette-Teller (BET) linear equation in the approximate p/p_0 relative pressure within the range of 0.1–0.3. Total pore volumes were calculated based on the final adsorption point. Barrett, Joyner and Halenda (BJH) methodology was used to determine the pore size distributions from adsorption branch of the isotherms.

Phase composition of as prepared and spent catalysts were determined using X-Ray diffraction spectroscopy (XRD). XRD analyses were carried out using Rigaku Intelligent X-Ray diffraction system SmartLab equipped with a sealed tube X-Ray generator (a copper target; operated at 40 kV and 15 mA), a D/teX high-speed position sensitive detector system. Conditions for obtaining data: 2θ range 5–80°, scan step 0.01 and scan speed 1°/min. The Scherrer constant was equal to 0.891. Optimization of obtained spectra was performed using a pseudo-Voight function. Rigaku PDXL software was used for analysis of crystal structure. The identification of all X-ray powder diffraction curves was performed using the COD database as a reference.

TGA patterns were detected by a METTLER TOLEDO thermogravimetric analyzer in order to investigate carbon deposits formation on spent catalysts. The catalyst sample was heated from 25° to 950°C with heating rate 10 °C/min, in flow of 40 ml/min of air. For reference, also TGA patterns of fresh catalysts were detected.

Surface composition analysis was performed using X-ray excited photoelectron spectroscopy (XPS). The analysis was performed based on the survey spectra and the spectra of the regions for the selected elements. A multi-chamber UHV analytical system, Prevac, equipped with a VG Scienta SAX 100 X-ray tube and an aluminum anode equipped with a VG Scienta XM 780 monochromator emitting radiation with a characteristic line of Al Kα and energy of 1486.6 eV was used for the measurements. The apparatus was equipped with a photoelectron energy analyzer (Scienta R4000). Pressure in the analysis chamber: not higher than 1.0E-8 mbar.

The surface morphology was evaluated using microscopic imaging in bright field scanning transmission microscopy (BF-STEM) mode, mapping of the distribution of individual elements, and selective area electron diffraction (SAED) analysis together with fast Fourier transform (FFT) analysis for the most active catalytic sample. The analysis was performed using a high-resolution electron microscope Titan G2 60–300 kV (FEI). The microscope was equipped with a field emission (FEG) gun, monochromator, three-lens condenser system, objective lens system, image corrector (Cs corrector), HAADF detector, and EDS spectrometer (Energy Dispersive X-Ray Spectroscopy Electron beam accelerating voltage of 300 kV. The sample preparation for the analysis

MOST WIEDZY Downloaded from mostwiedzy.pl

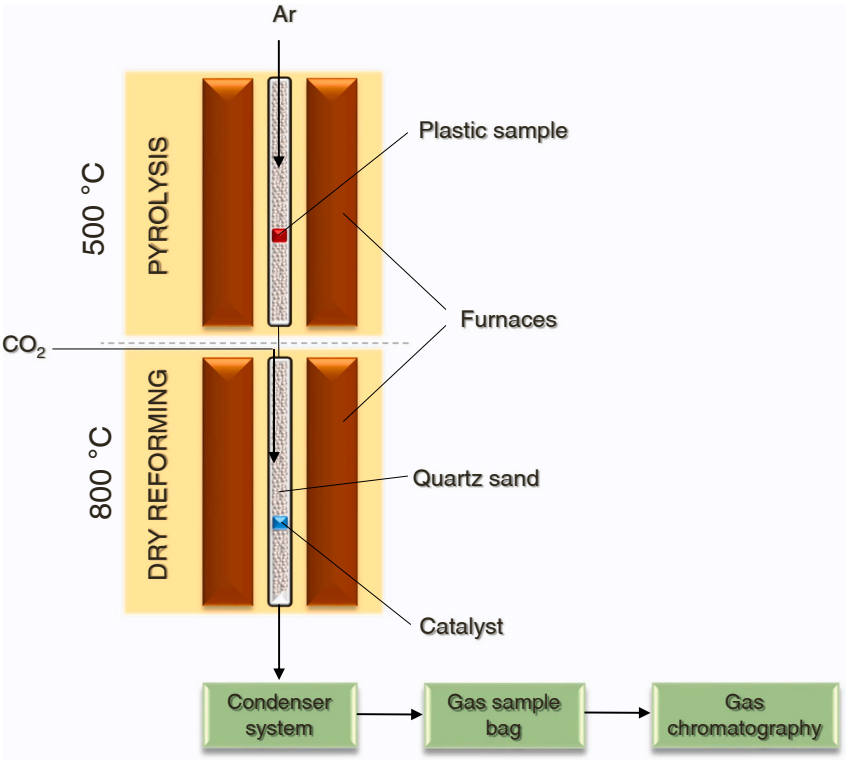

Fig. 2. Experimental set-up for pyrolysis combined with dry reforming process.

Table 1
Product yields, H_2:CO molar ratio and CO_2 conversion in the pyrolysis combined with dry reforming of LDPE with different catalyst.

Catalyst	No catalyst	Ni/$MgAl_2O_4$	Ni-TiC/$MgAl_2O_4$	Ni-Mo_2C/$MgAl_2O_4$	Ni-WC/$MgAl_2O_4$
Syngas yield [mmol/$g_{plastic}$]	38.55	79.38	80.44	69.13	81.84
H_2 yield [mmol/$g_{plastic}$]	12.69	30.63	28.30	25.59	23.43
CO yield [mmol/$g_{plastic}$]	25.87	48.75	52.15	43.53	58.41
CH_4 yield [mmol/$g_{plastic}$]	3.72	3.63	3.75	1.63	0.64
H_2:CO molar ratio	0.49	0.63	0.54	0.59	0.40
CO_2 conversion [g/$g_{plastic}$]	2.41	3.45	3.36	2.27	1.70

Table 2
Product yields, H_2:CO molar ratio and CO_2 conversion in the pyrolysis combined with dry reforming of PS with different catalyst.

Catalyst	No catalyst	Ni/$MgAl_2O_4$	Ni-TiC/$MgAl_2O_4$	Ni-Mo_2C/$MgAl_2O_4$	Ni-WC/$MgAl_2O_4$
Syngas yield [mmol/$g_{plastic}$]	14.38	38.81	54.90	57.27	26.91
H_2 yield [mmol/$g_{plastic}$]	3.96	10.55	13.66	16.27	14.64
CO yield [mmol/$g_{plastic}$]	10.41	28.26	41.25	41.00	12.27
CH_4 yield [mmol/$g_{plastic}$]	0.62	0.49	0.56	0.54	1.10
H_2:CO molar ratio	0.38	0.37	0.33	0.40	1.19
CO_2 conversion [g/$g_{plastic}$]	1.65	2.16	2.79	2.44	2.57

consisted of grinding in a mortar, followed by slurrying and homogenization in anhydrous ethanol. The suspension containing the sample was pipetted and placed on copper grids (200 mesh in 200 mesh) covered with lacey formvar stabilized with carbon (Ted Pella) and left on paper for ethanol evaporation.

2.3. Catalytic activity

Catalytic activity of catalysts was examined during pyrolysis combined with dry reforming of model materials that linger in the environment: low-density polyethylene (LDPE) and polystyrene (PS). PCDR processes were performed in the two-stage reactor system presented in Fig. 2. The experimental setup comprised two separate fixed-bed reactors, each equipped with its own furnace. Argon (50 ml/min) was fed into the top of the first stage reactor and carbon dioxide (50 ml/min) was fed into the top of second stage reactor. The dry reforming reactor was preheated before the pyrolysis stage reactor and maintained at a consistent temperature of 800 °C. Subsequently, the pyrolysis stage reactor was gradually heated at a rate of 10 °C/min until it reached a temperature of 500 °C, where it was sustained for a duration of 30 min. The resultant pyrolysis gases were directly introduced into the dry reforming stage reactor, in which catalyst was placed. Catalyst to plastic mass ratio was equal to 0.5. The generated gases were cooled through a condenser setup, comprising one condenser operating at room temperature and another condenser cooled by dry ice. This arrangement effectively captured any condensable liquids. The resulting uncondensed gas products were collected in a 25 L gas sample bag. Subsequently, gas analysis was conducted using gas chromatography (Clarus

MOST WIEDZY Downloaded from mostwiedzy.pl

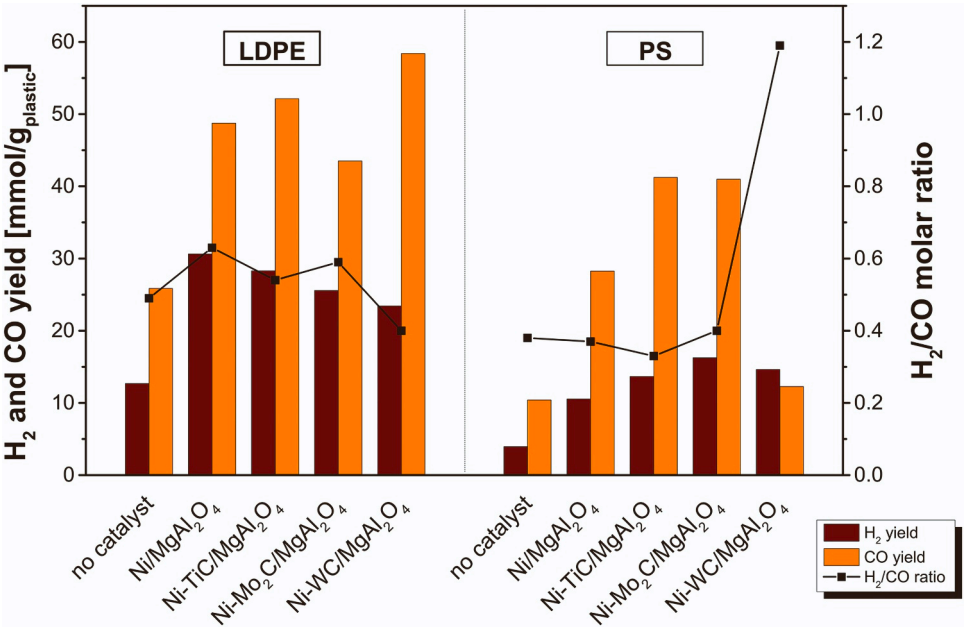

Fig. 3. Syngas (H_2 and CO) yield and composition in the pyrolysis combined with dry reforming (800 °C) of LDPE and PS over different catalyst.

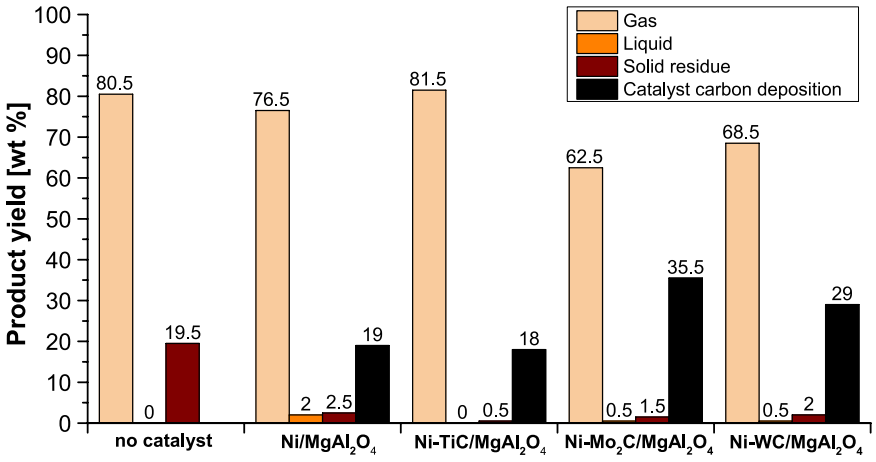

Fig. 4. Product distribution in the pyrolysis combined with dry reforming (800 °C) of LDPE with different catalyst.

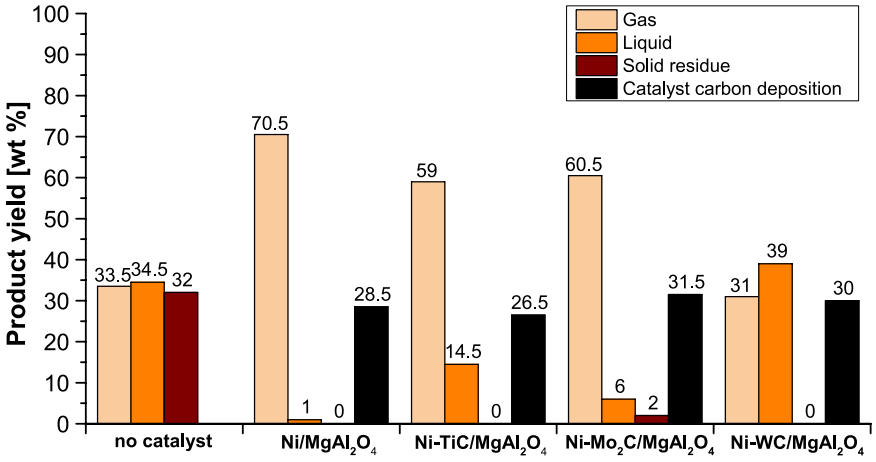

Fig. 5. Product distribution in the pyrolysis combined with dry reforming (800 °C) of PS with different catalyst.

MOST WIEDZY Downloaded from mostwiedzy.pl

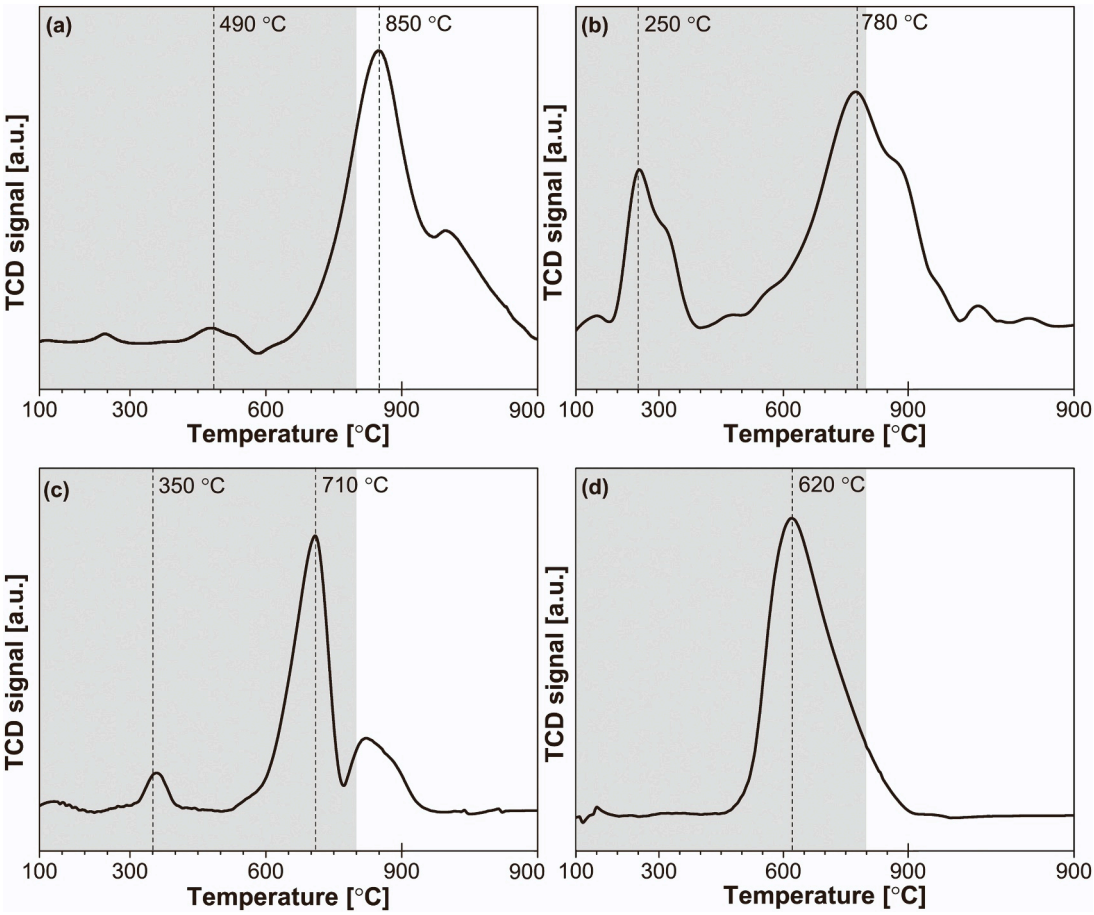

Fig. 6. H_2-TPR profiles for the obtained catalysts: (a) Ni/$MgAl_2O_4$; (b) Ni-TiC/$MgAl_2O_4$; (c) Ni-Mo_2C/$MgAl_2O_4$; (d) Ni-WC/$MgAl_2O_4$.

590, PerkinElmer) with thermal conductivity detection. Total amount of CO_2 introduced into the system was calculated from the known flow rates. Carbon dioxide conversion was determined as gram per gram of plastic sample according to the formula shown below:

$$X_{CO_2} = \frac{[m_{CO_2}]_{in} - [m_{CO_2}]_{out}}{[m_{plastic}]_{in}} \quad (2)$$

where $[m_{CO2}]_{in}$ is the weight of carbon dioxide introduced into the system [g], $[m_{CO2}]_{out}$ is the weight of carbon dioxide in the gas sample bag [g], and $[m_{plastic}]_{in}$ is the weight of the plastic sample.

In order to determine detailed composition of feedstock in the dry reforming, standalone pyrolysis processes were carried out in 500 °C under Ar flow of 50 ml/min. Output gaseous and liquid products obtained in pyrolysis of LDPE and PS were analyzed using gas chromatography-mass spectrometry technique. Volatile compound extraction was conducted utilizing headspace solid-phase microextraction (HS-SPME). Before extraction, liquid samples were subjected to a heating process at 40 °C for 2 min and agitated at a speed of 650 rpm. Before every injection, the fiber was desorbed at 250 °C for 5 min within a specialized desorption apparatus. The extraction process was executed at 40 °C for a span of 50 min, employing a divinylbenzene/carboxen/polydimethylsiloxane (DVB/CAR/PDMS) SPME fiber with dimensions of 50/30 μm in thickness and 1 cm in length, procured from Merck Co., New York, USA. Subsequent to extraction, the fiber was carefully retracted from its vial and introduced into a gas chromatograph's injector for the thermal desorption of analytes at 250 °C for 200 s. This was followed by a secondary desorption within the desorption apparatus at 250 °C for 5 min. For extractions involving Tedlar bags, the SPME fiber was positioned within the Tedlar bag port, puncturing the membrane, and thus allowing the fiber to be exposed to the analytes.

The employed GC system incorporated an Agilent 6890 A gas chromatograph (Agilent Technologies, Palo Alto, CA, USA) interfaced with a Pegasus IV time-of-flight mass spectrometer (LECO Corp., St. Joseph, MI, USA). The column configuration comprised a 30 m x 0.25 mm× 1 μm column with an Equity1 stationary phase (Supelco Co., Bellefonte, Pennsylvania, USA) and a protective 0.5 m x 0.1 mm guard column (Restek, Bellefonte, Pennsylvania, USA). Compound separation within the samples was attained via an optimized temperature program: commencing at 35 °C (maintained for 2 min) and then escalating at 4 °C/min to a plateau of 250 °C, sustained for an additional 2 min. The entire analysis duration was approximated 60 min. The ion source was set at 250 °C, while the detector voltage was adjusted to − 1647 V. Analyzed ions ranged from m/z 18–450 at a deliberately slow data acquisition rate of 10 spectra/s, augmenting method sensitivity. For liquid samples, a multitask autosampler MPS II (Gerstel Co., Mülheim an der Ruhr, Germany) was integrated to ensure consistent sample handling and dosing conditions. Data processing was manually executed utilizing the ChromaTOF software's peak deconvolution program (LECO Corp., version 4.51.6.0). Tentative analyte identification was ascertained through an MS library search using the NIST 2011 and Wiley 2010 libraries. A pivotal selection criterion for peaks was a comparative metric delineating the congruence of a specific chromatographic peak's mass spectrum with the reference database spectrum. Employing a minimal threshold for signal-to-noise ratios enabled the recognition of a substantial count of chromatographic peaks, thus permitting the detection of trace compounds. The GC×TOFMS technique, combined with the peak deconvolution algorithm, greatly assisted in the provisional identification of compounds present in both liquid and gaseous sample volatile fractions under scrutiny.

MOST WIEDZY Downloaded from mostwiedzy.pl

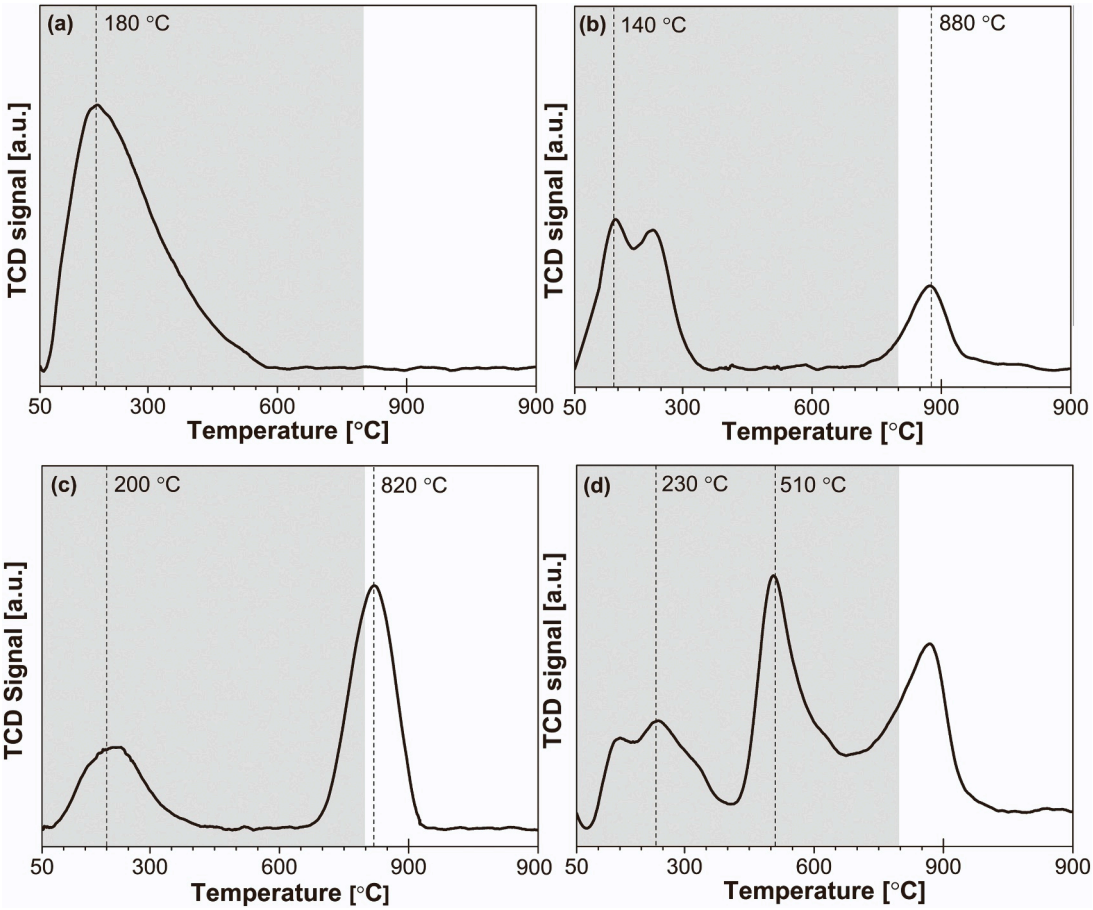

Fig. 7. CO_2-TPD for the obtained catalysts: a) $Ni/MgAl_2O_4$; (b) $Ni\text{-}TiC/MgAl_2O_4$; (c) $Ni\text{-}Mo_2C/MgAl_2O_4$; (d) $Ni\text{-}WC/MgAl_2O_4$.

Table 3
BET surface area and total pore volume for catalysts before and after PCDR and total basicity of fresh catalysts.

Catalyst	BET surface area [m^2/g]			Total pore volume [cm^3/g]			Total basicity [$mmol_{CO2}/g$]
	Fresh catalyst	Catalyst after PCDR of LDPE	Catalyst after PCDR of PS	Fresh catalyst	Catalyst after PCDR of LDPE	Catalyst after PCDR of PS	
$MgAl_2O_4$	74 ± 4	-	-	0.37 ± 0.02	-	-	-
$Ni/MgAl_2O_4$	71 ± 4	15 ± 1	79 ± 4	0.36 ± 0.02	0.07 ± 0.01	0.23 ± 0.01	0.036
$Ni\text{-}TiC/MgAl_2O_4$	68 ± 3	45 ± 2	53 ± 3	0.31 ± 0.02	0.19 ± 0.01	0.15 ± 0.01	0.028
$Ni\text{-}Mo_2C/MgAl_2O_4$	70 ± 4	56 ± 3	43 ± 2	0.27 ± 0.01	0.25 ± 0.01	0.18 ± 0.01	0.037
$Ni\text{-}WC/MgAl_2O_4$	163 ± 8	48 ± 2	23 ± 1	0.24 ± 0.01	0.17 ± 0.01	0.11 ± 0.01	0.055

3. Results

3.1. Catalytic activity

The catalytic activity of the catalysts was examined in pyrolysis combined with dry reforming of two different plastic feedstocks: LDPE and PS. The composition of gas and liquid products obtained from the standalone pyrolysis process, which was the feedstock in the dry reforming stage, was characterized using gas chromatography–mass spectrometry technique. Obtained chromatograms and detailed tables containing the list of identified compounds present in the pyrolysis output stream are presented in Supplementary Data (Fig. S1 and Tab. S1 for LDPE and Fig. S2 and Tab. S2 for PS). In the case of pyrolysis of low density polyethylene, a number of various aliphatic, cyclic and aromatic hydrocarbons of a carbon chain length in the range of C5-C20 were identified in the output stream. The potential emergence of C2-C4 compounds, encompassing alkanes, alkenes, and alkynes in the samples, can be inferred from the prominent abundance of specific *m/z* values such as 29, 43, and 57 at the chromatogram's lower retention times. The methodology employed does not confer the capability to unequivocally ascertain the presence of the aforementioned chemical entities due to the prevalent occurrence of the highlighted ionic fragments that can also correspond to many other substances. However, it is reported in the literature that random-chain scission mechanism, that occurs during the pyrolysis of LDPE, leads to wide spectrum of hydrocarbon products, including lower chain hydrocarbons as well [9,29–31]. On the other hand, the output stream of pyrolysis of polystyrene was composed mainly of styrene, which is PS monomer, and its oligomers. In addition, other benzene derivatives as well as aliphatic hydrocarbons (C6-C20) were identified. Presence of compounds containing N or O atoms, can be explained by the low content of these elements in LDPE and PS feedstock. Elemental analysis of plastic feedstock was performed

MOST WIEDZY Downloaded from mostwiedzy.pl

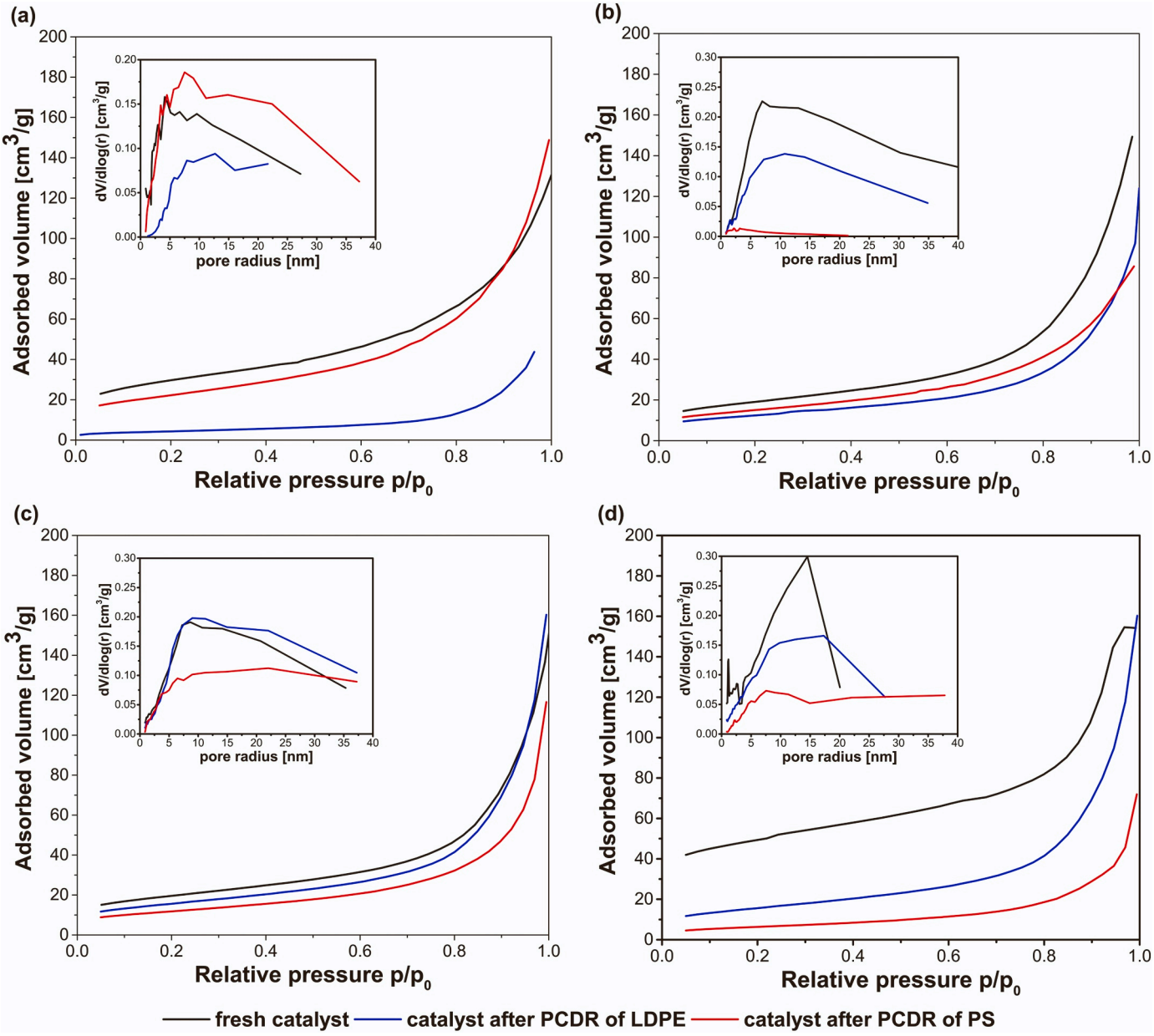

Fig. 8. Nitrogen adsorption isotherms and pore size distributions of catalysts before and after pyrolysis combined with dry reforming of LDPE and PS: a) Ni/$MgAl_2O_4$; (b) Ni-TiC/$MgAl_2O_4$; (c) Ni-Mo_2C/$MgAl_2O_4$; (d) Ni-WC/$MgAl_2O_4$.

in our previous work [32] and resulted in nitrogen content equal to 1.189% and 0.368% for LDPE and PS, while oxygen content was equal to 6.552% and 2.434% respectively. Moreover, oxygenated compounds may be obtained due to reactions with CO_2.

The product yields, CO_2 conversion, and syngas H_2:CO molar ratios obtained in PCDR over different catalysts are given in Tables 1 and 2 for the LDPE and PS feedstock, respectively. The H_2 yield, CO yield, and H_2:CO molar ratio are shown in Fig. 3. The product distributions for the PCDR of LDPE are shown in Fig. 4 and Fig. 5 for PCDR of PS. Non-catalytic PCDR processes were also performed for comparison.

PCDR processes carried out without a catalyst resulted in the lowest syngas yield equal to 38.55 mmol/g and 14.38 mmol/g for LDPE and PS feedstock, respectively. Syngas contained more hydrogen (12.69 mmol/g) when LDPE was used as a raw material. In the case of non-catalytic PCDR of PS, hydrogen yield was equal to 3.96 mm/g. Obtained results are in line with the literature indicating that the dry reforming of hydrocarbons is highly endothermic process and requires application of catalysts to reduce required thermal energy and to obtain acceptable syngas yield [12,13]. It should be noted that quartz sand can include trace quantities of metal impurities that may serve as catalysts for reforming reactions [30].

According to the presented results, all catalytic processes resulted in significantly higher syngas yields than PCDR carried out without a catalyst. In the case of PCDR of LDPE (Table 1), modification with TiC and WC resulted in higher syngas yields (80.44 and 81.84 mmol/g, respectively) than for unmodified catalyst (79.38 mmol/g). In contrast, modification with Mo_2C resulted in a lower syngas yield (69.13 mmol/g). The highest syngas yield equal to 81.84 mmol/g was observed in the PCDR using the Ni-WC/$MgAl_2O_4$ catalyst. The modification of the catalyst also affected the H_2:CO ratio of the obtained syngas. H_2:CO ratio increased as follows: Ni-WC/$MgAl_2O_4$ <Ni-TiC/$MgAl_2O_4$ <Ni-Mo_2C/$MgAl_2O_4$ <Ni$MgAl_2O_4$.

The synthesis gas yields for PCDR of PS were lower compared to LDPE. As it is presented in Table 2, Ni-TiC/$MgAl_2O_4$ and Ni-Mo_2C/

MOST WIEDZY Downloaded from mostwiedzy.pl

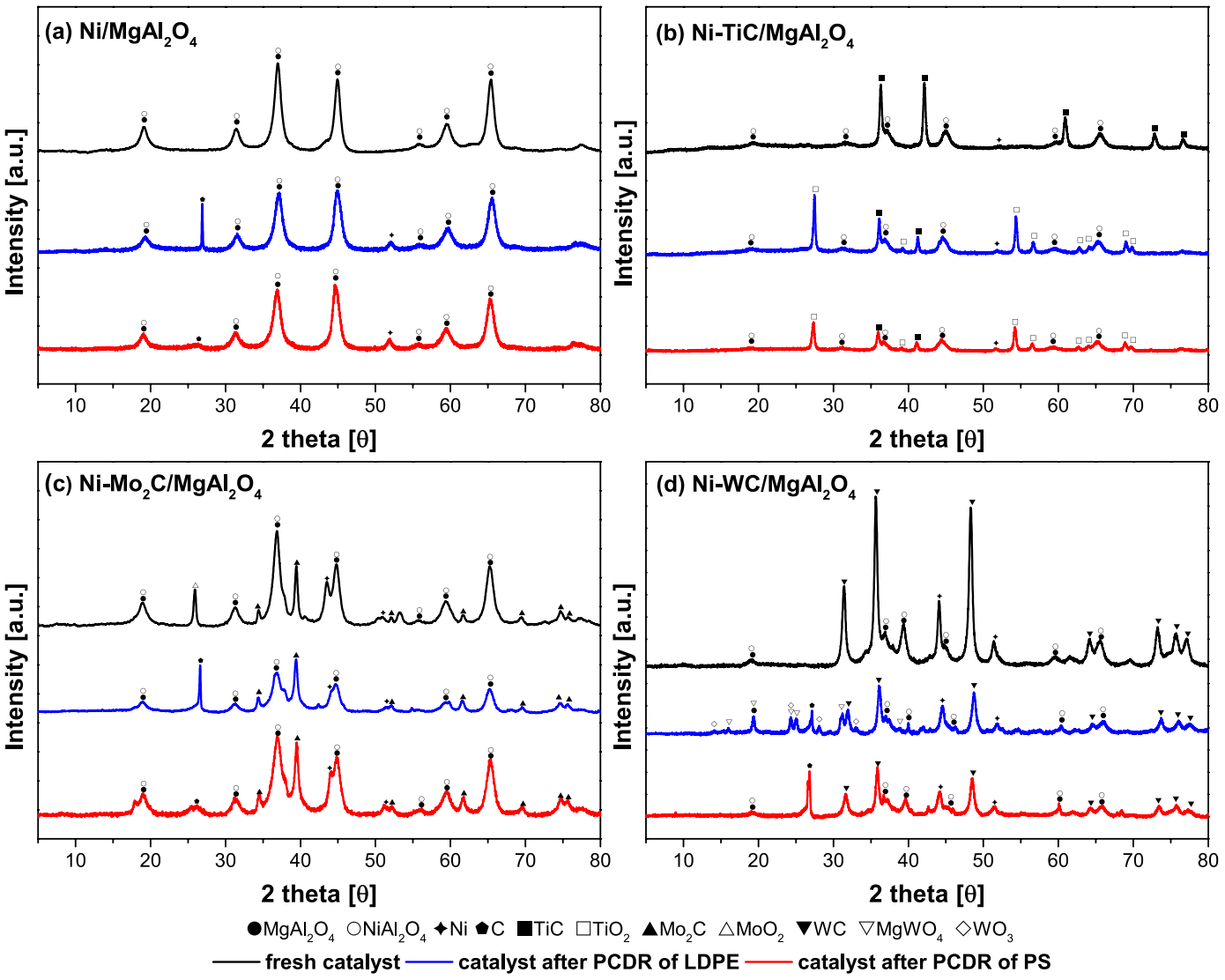

Fig. 9. XRD patterns for the obtained and spent catalysts: a) $Ni/MgAl_2O_4$; (b) $Ni\text{-}TiC/MgAl_2O_4$; (c) $Ni\text{-}Mo_2C/MgAl_2O_4$; (d) $Ni\text{-}WC/MgAl_2O_4$.

$MgAl_2O_4$ exhibited higher syngas yield (54.90 mmol/g and 57.27 mmol/g, respectively) than unmodified catalyst (38.81 mmol/g), whereas in the case of WC-modified catalyst syngas yield was lower, equal to 26.91 mmol/g. Considering syngas composition, H_2:CO ratio increased as follows: $Ni\text{-}TiC/MgAl_2O_4$ <$Ni/MgAl_2O_4$ <$Ni\text{-}Mo_2C/MgAl_2O_4$ <$Ni\text{-}WC/MgAl_2O_4$.

As presented in Figs. 4 and 5 product distribution varied depends on the used feedstock. In the case of PS more liquid fraction appeared compared to LDPE. Moreover, in PCDR of polystyrene feedstock, greater amount of carbon deposits was formed, which is consistent with TG analysis (Section 3.2). It was observed that modification of catalyst with different metal carbide resulted in different product distribution. For PCDR of LDPE carried out over modified catalysts, amount of liquid fraction decreased compared to unmodified catalyst from 2% to 0%, 0.5% and 0.5% for catalyst modified with TiC, Mo_2C and WC, respectively. In the case of PCDR carried out with PS as feedstock opposite tendency was observed – amount of liquid fraction was greater (14.5%, 6%, 39% for $Ni\text{-}TiC/MgAl_2O_4$, $Ni\text{-}Mo_2C/MgAl_2O_4$ and $Ni\text{-}WC/MgAl_2O_4$, respectively) than process carried out over unmodified catalyst (1%). Considering carbon deposition, the most promising catalyst turned out to be $Ni\text{-}TiC/MgAl_2O_4$, in which case both in PCDR of LDPE and PCDR of PS, carbon deposition decreased (18% and 26.5%, respectively) compared to unmodified catalyst (19% and 28.5% respectively).

The above-mentioned differences in the distribution of products for individual processes may result from different ways of polymer decomposition at the pyrolysis stage, thus different hydrocarbons generated for dry reforming stage as well as different reaction mechanisms for nickel and nickel-carbide catalysts. According to literature, during the pyrolysis of PS, large polymer molecules break up by random scission and chain-end scission into small aromatic molecules (mainly styrene and its oligomers) [9,33]. Subsequently, aromatic hydrocarbons might take a part in oligomerisation reactions, resulting in transformation into polycyclic aromatics, that are part of the liquid fraction. Moreover, polycyclic aromatic compounds are also coke precursors, which may explain the formation of amorphous carbon in PCDR of PS [34]. In contrast, when dealing with polyolefins like LDPE, during pyrolysis more low molecular gaseous hydrocarbons such as C_2-C_3 alkanes and alkenes are generated, which undergo dry reforming reactions in the next stage [9]. Besides the conversion to syngas, these hydrocarbons can also be involved in the generation of carbon deposits. In contrast to the aromatic hydrocarbons generated in the case of PS, they are less stable and not as sterically hindered, hence they more easily participate in the formation of graphitic than amorphous forms of carbon [34].

MOST WIEDZY Downloaded from mostwiedzy.pl

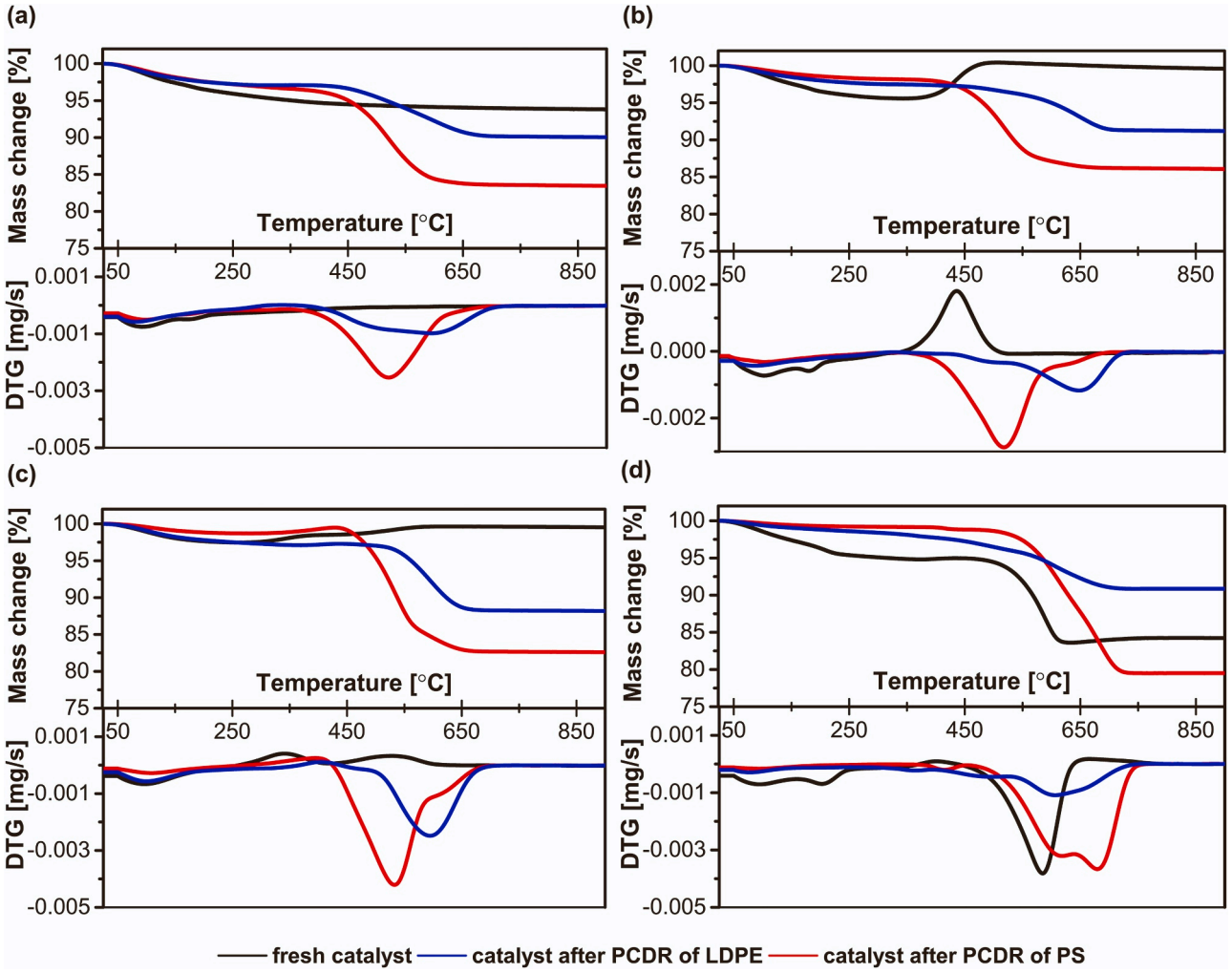

Fig. 10. TG and DTG curves for the obtained and spent catalysts: a) Ni/$MgAl_2O_4$; (b) Ni-TiC/$MgAl_2O_4$; (c) Ni-Mo_2C/$MgAl_2O_4$; (d) Ni-WC/$MgAl_2O_4$.

3.2. Catalyst characterization

To evaluate the influence of metal carbides on reducibility, metal-support interactions and basicity of the catalysts, temperature-programmed reduction (H_2-TPR) and desorption (CO_2-TPD) analyses were conducted. It should be noted that temperature region that should be given the most attention is up to 800 °C (area marked grey in the Figs. 6–7), at which catalyst was previously calcined. It is due to the possible other changes of catalyst structure that may occur at temperatures higher than its calcination. Analyses were extended up to 900 °C in order to investigate changes in the case of possible local overheating. However, no significant changes in the TPR and TPD curves were observed that clearly started after exceeding the 800 °C boundary - only those changes that started before reaching this temperature were progressing.

The H_2-TPR profiles of the obtained catalysts are shown in Fig. 6(a-d). In the case of the Ni-$MgAl_2O_4$ catalyst, two distinct reduction peaks were observed. The first peak, occurring at lower temperatures (440–570 °C), was assigned to the reduction of NiO particles with relatively weak interactions with the catalyst support. The second peak, situated at higher temperatures (660–900 °C), corresponded to the reduction process of strongly interacting Ni species within the $NiAl_2O_4$ phase or NiO [35–37]. For the Ni-TiC/$MgAl_2O_4$ and Ni-Mo_2C/$MgAl_2O_4$ catalysts, the reduction peaks exhibited a shift towards lower temperatures. For Ni-TiC/$MgAl_2O_4$ catalyst peaks were shifted to 180–370 °C and 570–900 °C respectively, whereas for Ni-Mo_2C/$MgAl_2O_4$ sample shift was slighter (300–400 °C and 580–900 °C). It should be noted that peaks related to the presence of additional oxides owing to the passivation process may also occur. According to literature reports, in the region of 570–650 °C overlapped peaks corresponding to TiO_2 reduction [38–40] may be present, and at 300–400 °C and 600–800 °C overlapped peaks related to the reduction of MoOx species [41–43]. The modification of the Ni-$MgAl_2O_4$ catalyst with tungsten carbide resulted in only one peak in the temperature range of 500–890 °C. This peak may also overlap with the signal corresponding to the reduction of WOx oxides, which can be observed in the 600–900 °C region [44–46].

The basicity of the catalysts was evaluated using CO_2-TPD. The catalytic properties are anticipated to improve due to the presence of strong basicity, resulting in enhanced CO_2 adsorption. The obtained CO_2-TPD profiles are shown in Fig. 7(a-d). The total basicity of the catalysts, estimated from the integration of CO_2-TPD peaks, is summarized in Table 3. All samples exhibited strong and broad desorption peaks in the temperature range of 50–450 °C, which can be attributed to chemisorbed CO_2 over basic sites with weak and moderate intensities. The modification of Ni/$MgAl_2O_4$ with metal carbides resulted in additional peaks related to the strong basic sites. The Ni-TiC/$MgAl_2O_4$ sample exhibited a second desorption peak at temperatures in the range from 760° to 900°C. Although the strength of the basic sites increased, the total basicity decreased to 0.028 mmol/g. For Ni-Mo_2C/$MgAl_2O_4$ strong sites related peak appeared at temperature of 710–900 °C and the total basicity was slightly increased to 0.037 mmol/g. The Ni-WC/$MgAl_2O_4$ catalyst exhibited the highest total basicity (0.055 mmol/g). In

MOST WIEDZY Downloaded from mostwiedzy.pl

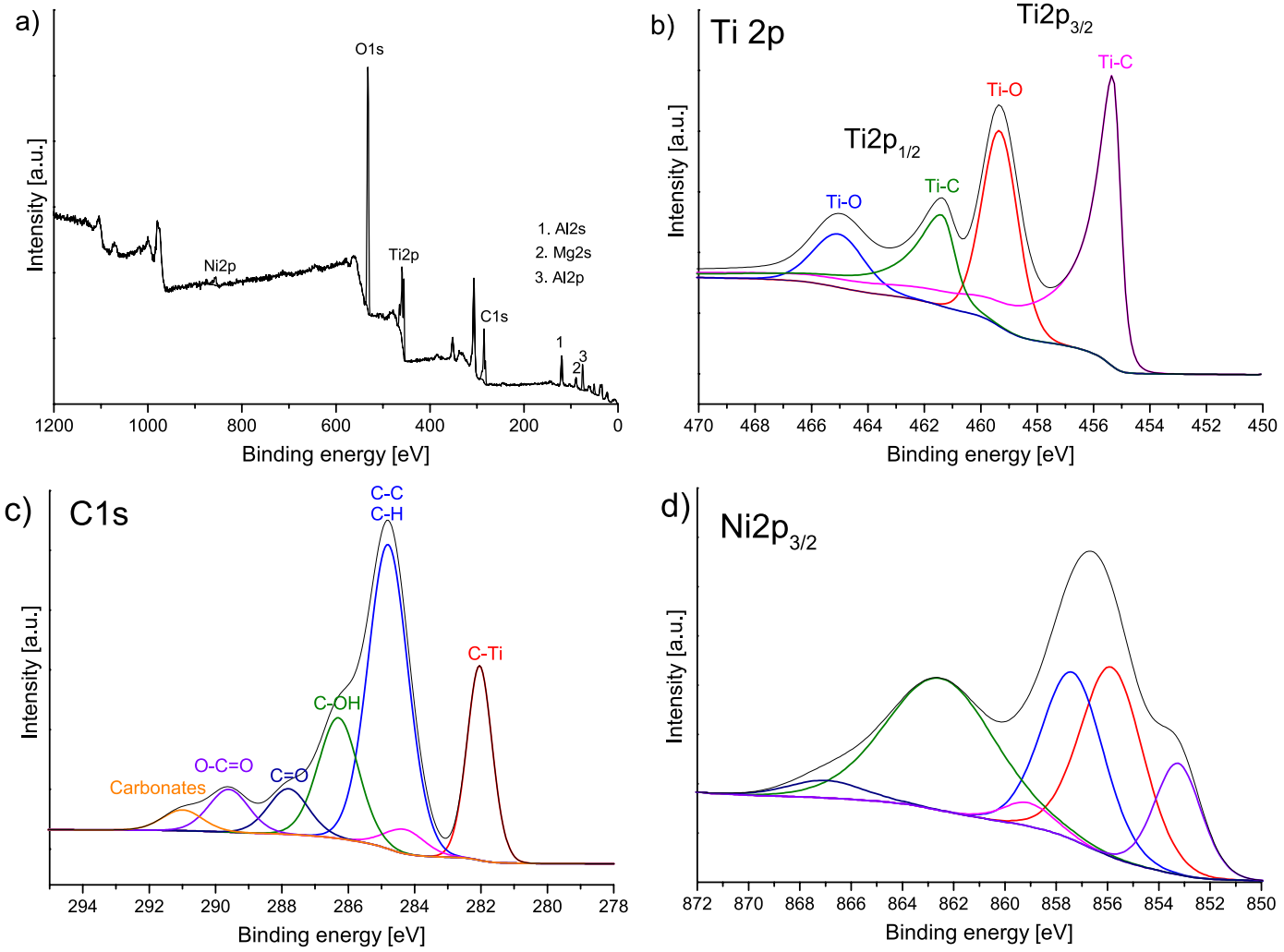

Fig. 11. XPS spectra of Ni-TiC/$MgAl_2O_4$ catalyst a) survey spectrum, b) Ti 2p region, c) carbon 1 s region and d) $Ni2p_{3/2}$ region.

addition, a broad desorption peak at temperatures from 420° to 900°C indicates the enhanced strength of the basic sites.

The results of the BET surface analysis are shown in Table 3. For Ni/$MgAl_2O_4$, BET surface area and total pore volume was equal to 71 m^2/g and 0.36 cm^3/g respectively. The values did not differ significantly compared to $MgAl_2O_4$ support. Carbide-modified catalysts resulted in slightly lower total pore volumes than the unmodified catalysts. After the catalytic reactions, the total pore volumes of all catalysts declined, and the decline was higher in the case of the PCDR of PS in comparison to that of LDPE. This decline can be related to the deactivation of the catalyst, which could stem from processes such as sintering or the deposition of coke. Modification of the nickel catalyst with titanium and molybdenum carbides did not cause a significant impact on the surface area (68 ± 3 and 70 ± 4 m^2/g, respectively), whereas Ni-WC/$MgAl_2O_4$ showed the highest BET specific surface area of 163 ± 8 m^2/g. The enhanced surface area indicates an increased number of active sites and a greater availability of reactants, which may contribute to better catalytic activity. Although the obtained Ni-WC/$MgAl_2O_4$ catalyst showed a high specific surface area, the BET surface area decreased to 48 ± 2 m^2/g and 23 ± 1 m^2/g after the PCDR of LDPE and PS, respectively. A similar tendency was observed for Ni-Mo_2C/$MgAl_2O_4$, where the BET surface area decreased after both catalytic processes, and the decrease was greater for PS as a raw material. After pyrolysis combined with dry reforming over the Ni-TiC/$MgAl_2O_4$ catalyst, the BET surface area decreased as well; however, unlike in the case of the molybdenum and tungsten carbide-modified catalysts, the decrease was greater after the PCDR of LDPE. After the PCDR of LDPE over unmodified Ni/$MgAl_2O_4$, the BET surface area of the catalyst decreased to 15 ± 1 m^2/g, whereas after the PCDR of PS, the BET surface area slightly increased to 79 ± 4 m^2/g.

Catalysts nitrogen adsorption isotherms and pore size distributions are shown in Fig. 8. For all examined fresh and spent catalysts, the shape of the depicted curves aligns with the H1 hysteresis loop and IV type of classified isotherms [47,48]. In the case of unmodified catalyst, pores with a radius of 2–15 nm predominate (centred at 4 nm), indicating a mesoporous structure. After modification of catalyst the highest peak was shifted to 7 nm, 9 nm and 15 nm for catalyst modified with TiC, Mo_2C and WC respectively. Modification with molybdenum and titanium carbides resulted in the additional presence of macropores in the radius range of 25–35 and 25–40 nm respectively. Besides both processes over Ni-TiC/$MgAl_2O_4$ and PCDR of LDPE over Ni$MgAl_2O_4$, tendency of increased range of pores was observed for spent catalysts. It can be explained by presence of additional compounds formed in the PCDR reaction, such as carbon deposits or oxides. In contrast, BJH analysis for spent Ni-TiC/$MgAl_2O_4$ and Ni/$MgAl_2O_4$ after PCDR of LDPE indicated narrower pore range than as-prepared catalysts, which may be due to clogging by coke deposits or sintering.

The XRD patterns of the obtained and spent catalysts are shown in Fig. 9(a-d). A spinel $MgAl_2O_4$ crystal phase was observed in all catalyst samples (reference card CSD: data_1010129 (COD)). The reflections observed at $2\theta = 19.2°$, 31.6°, 36.9°, 44.9°, 55.8°, 59.5° and 65.4° correspond to the spinel (1 1 1), (2 2 0), (3 1 1), (4 0 0), (4 2 2), (4 0 4),

MOST WIEDZY Downloaded from mostwiedzy.pl

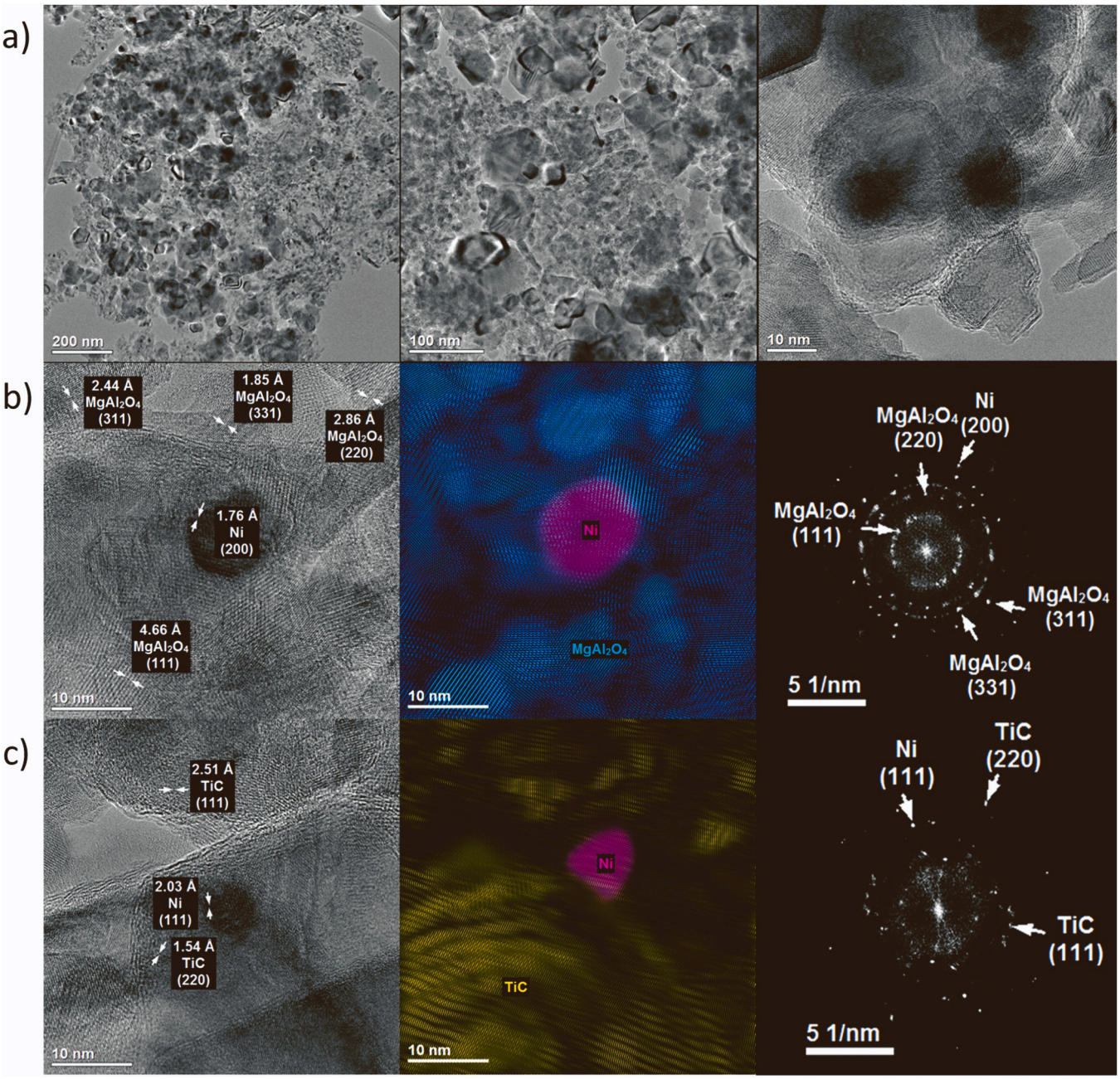

Fig. 12. BF-TEM images of Ni-TiC/$MgAl_2O_4$ catalyst a) overall view, b) identification of $MgAl_2O_4$ and Ni, c) identification of Ni and TiC phases.

and (5 3 3) crystal phases, respectively. XRD pattern of $MgAl_2O_4$ support is included in the Supplementary Data for reference (see Fig. S3). No discernible peaks corresponding to nickel oxide species were detected in the Ni-$MgAl_2O_4$ catalyst. This observation suggests the possibility of nickel oxide being present in small sizes, well-dispersed NiO, or potential doping with $MgAl_2O_4$. The locations of the reflections assigned to MgAl2O4 coincide with those associated with $NiAl_2O_4$, which could form at elevated temperatures (such as the calcination temperature of 800 °C). This formation might occur as a consequence of a solid-state reaction between NiO and $MgAl_2O_4$. [35]. In our previous work, we performed a more detailed characterization that indicated partial formation of $NiAl_2O_4$ phase [49].

The XRD patterns of the spent Ni/$MgAl_2O_4$ after both catalytic processes (Fig. 9a) indicate the deposition of carbon on the catalyst. For the catalyst after PCDR, the PS halo at $2\theta = 26.4°$ is observed, which may be related to the deposited amorphous carbon [50–52], while in the case of the PCDR of LDPE, an additional diffraction peak attributed to graphitic carbon (reference card CSD: data_120017 (COD)) were observed at $2\theta = 26.9°$. In the case of Ni-TiC/$MgAl_2O_4$ catalyst (Fig. 9b) additional peaks at $2\theta = 36.3°$, 42.1°, 60.9°, 72.8°, 76.6° corresponding to TiC phase were observed (reference card CSD: 5910091 (COD)). The diffraction peaks at $2\theta = 27.5°$, 39.2°, 54.6°, 56.7°, 62.8°, 64.1°, 69.0°, 69.8° in XRD pattern of spent Ni-TiC/$MgAl_2O_4$ catalyst, correspond to TiO_2 rutile phase indicating partial oxidation of the catalyst. For Ni/$MgAl_2O_4$ modified with Mo_2C, additional peaks were observed at $2\theta = 34.4°$, 39.5°, 52.1°, 61.7°, 69.5°, 74.5°, and 75.8°, corresponding to Mo_2C (reference card CSD: mp-1221498) (Fig. 9c). The peak observed at $2\theta = 25.9°$ may be related to the MoO_2 phase (reference card CSD: mp-1761012) due to the passivation process after the synthesis of the catalyst. The diffraction peak at $2\theta = 26.6°$ in the XRD pattern of the spent Ni-Mo_2C/$MgAl_2O_4$ catalyst after PCDR of LDPE may correspond to graphitic carbon. In the case of PCDR of PS over the Ni-Mo_2C/$MgAl_2O_4$,

MOST WIEDZY Downloaded from mostwiedzy.pl

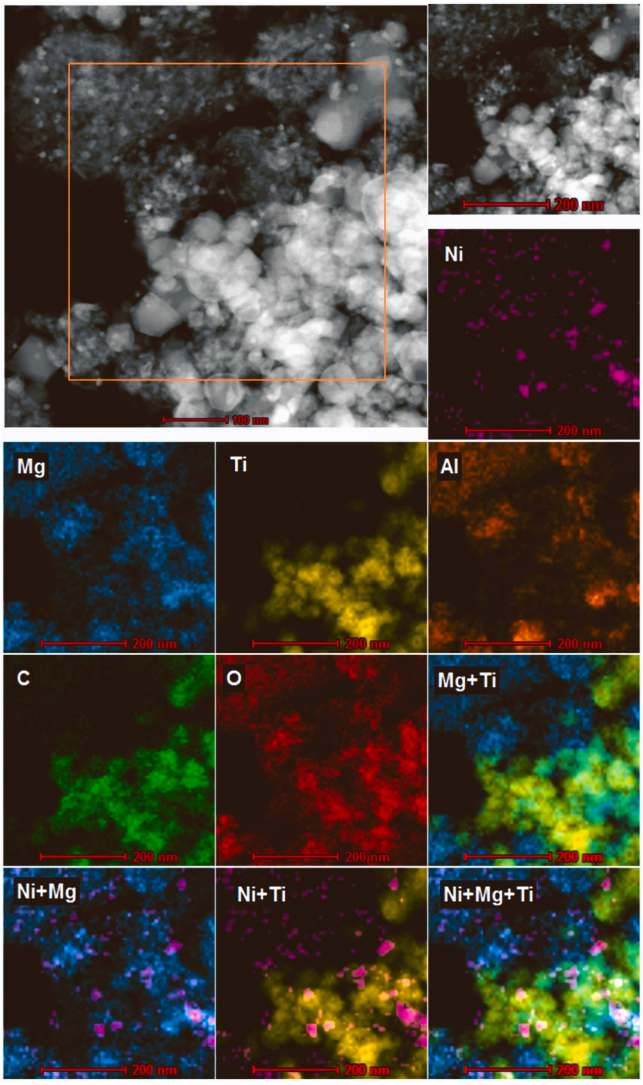

Fig. 13. EDS mapping of Ni-TiC/$MgAl_2O_4$ catalyst.

Table 4
Effect of reforming temperature on product yields, H_2:CO molar ratio and CO_2 conversion in the pyrolysis combined with dry reforming of LDPE carried out over $NiMgAl_2O_4$ catalyst.

Temperature	700 °C	750 °C	800 °C
Syngas yield [mmol/$g_{plastic}$]	36.61	64.45	79.38
H_2 yield [mmol/$g_{plastic}$]	13.05	21.14	30.63
CO yield [mmol/$g_{plastic}$]	23.56	43.31	48.75
CH_4 yield [mmol/$g_{plastic}$]	2.66	5.10	3.63
H_2:CO molar ratio	0.55	0.49	0.63
CO_2 conversion [g/$g_{plastic}$]	4.52	2.92	3.45

Table 5
Effect of reforming temperature on product yields, H_2:CO molar ratio and CO_2 conversion in the pyrolysis combined with dry reforming of LDPE carried out over Ni-TiC/$MgAl_2O_4$ catalyst.

Temperature	700 °C	750 °C	800 °C
Syngas yield [mmol/$g_{plastic}$]	65.92	66.44	80.44
H_2 yield [mmol/$g_{plastic}$]	21.58	22.24	28.30
CO yield [mmol/$g_{plastic}$]	44.34	44.20	52.15
CH_4 yield [mmol/$g_{plastic}$]	2.57	2.77	3.75
H_2:CO molar ratio	0.49	0.50	0.54
CO_2 conversion [g/$g_{plastic}$]	2.72	2.82	3.36

a halo around 2θ = 26.2° occurred in the XRD pattern of the used catalyst, which may correspond to deposited amorphous carbon [50–52]. For fresh Ni-WC/$MgAl_2O_4$ catalyst diffraction peaks at 2θ = 31.4°, 35.7°, 48.3°, 64.2°, 73.3°, 75.7°, 77.2° corresponding to WC phase (reference card CSD: 1501576 (COD)) were observed. In the XRD pattern of the reacted catalyst after the PCDR of LDPE, additional reflections were observed at 2θ = 16.0°, 19.4°, 24.3°, 25.0°, 31.2°, and 38.9°, and 2θ = 14.0°, 24.3°, 28.1°, 33.0°, attributed to $MgWO_4$ (reference card CSD: data_1010642 (COD)) and WO_3 (reference card CSD: data_1004057 (COD)) respectively. This was due to the partial oxidation of WC. Moreover, peak at 2θ = 27.1 was noticed, which may be related to formed graphitic carbon deposits on catalyst surface. In contrast, after the PCDR of PS, the only changes in the XRD pattern compared to the fresh catalyst were the peaks of graphitic carbon at 2θ = 26.9°.

The TG and DTG curves of as-prepared and catalysts after PCDR are presented in Fig. 10(a-d). The weight decrease observed for all samples during the temperature span of 50–180 °C can be attributed to the release of moisture content. For Ni/$MgAl_2O_4$ catalyst (Fig. 10a), after the PCDR, there are additional DTG peaks with maximum rate of weight loss at 600 °C and 515 °C for spent catalyst after PCDR of LDPE and PS, respectively. It can be related to the combustion of different type carbon deposited on the catalysts, for PCDR of LDPE – graphitic carbon and for PCDR of PS – more unstable amorphous carbon. These results are in line with the results of XRD analysis (Fig. 9a) discussed previously. In the case of Ni-TiC/$MgAl_2O_4$ catalyst (Fig. 10b), for fresh catalyst the weight gain can be observed at temperature 380–500 °C which is related to oxidation of TiC component to TiO_2. After catalytic reactions weight loss from 350 °C was observed with maximum rate at 515 °C for PCDR of PS and 650 °C for PCDR of LDPE, related to oxidation of amorphous and graphitic carbon, respectively. In the case of catalyst modified with Mo_2C, weight gain region at temperature 300–550 °C is related to oxidation of Mo_2C spices to MoO_3. After the reactions, the weight gain attributed to Mo_2C oxidation is masked by great weight loss from 400 °C to 680 °C. For Ni-Mo_2C/$MgAl_2O_4$ after PCDR of PS weight loss rate was the highest in 430–580 °C zone, while for PCDR of LDPE in 520–670 °C. Therefore, it can be concluded that in PCDR of LDPE higher amount of graphitic carbon was deposited, while in PCDR of PS more amorphous carbon was formed, which was also presented in XRD patterns (Fig. 9c). For WC-modified catalyst before the reaction decrease in TG curve was noticed within the temperature span of 400–600 °C, which can be associated to amorphous carbon residue after the synthesis. After PCDR of LDPE weight loss decreased which is related to oxidation of carbon during the catalytic reaction. In contrast, after PCDR of PS weight loss was greater compared to fresh catalyst, which indicates formation of additional carbon deposits during catalytic reaction. Maximum weight loss rate is at 680 °C which may be attributed to greater amount of graphitic carbon.

XPS analysis was performed to investigate the surface composition of the Ni-TiC/$MgAl_2O_4$ catalyst XPS analysis was performed. XPS spectra confirmed the presence of Ti, Ni, O, Mg, Al, and C in the catalyst sample (Fig. 11a). The Ti region (Fig. 11b) was deconvoluted into two main regions: $Ti2p_{2/3}$ and $Ti2p_{1/2}$. These two regions were further deconvoluted into signals attributed to Ti-O and Ti-C bonds. Signals assigned to titanium bonded with carbon-forming titanium carbide were observed at 461. 3 eV and 455.3 eV, for $Ti2p_{1/2}$ and $Ti2p_{2/3}$, respectively. Ti–O bonds were also observed in the XPS spectra. The formation of Ti-O bonds observed in both the $Ti2p_{1/2}$ (465.1 eV) and $Ti2p_{3/2}$ (459.3 eV) regions indicates the partial oxidation of TiC to TiO_2 due to the exposure to air after the synthesis step [53,54]. C1s region spectrum is shown in Fig. 11c. The spectrum was deconvoluted into six component peaks. The two main peaks of the highest intensity were attributed to the Ti-C and C-C bondings at 282.0 eV and 284.8 eV, respectively [54]. Furthermore, the oxidized states of the carbon terminated with hydroxyl at 286.3 eV (C-OH), carbonyl (C═O) (287.9 eV, O-C═O groups (289.5 eV and carbonate groups (291.1 eV) were observed. Oxidation may be a result of

MOST WIEDZY Downloaded from mostwiedzy.pl

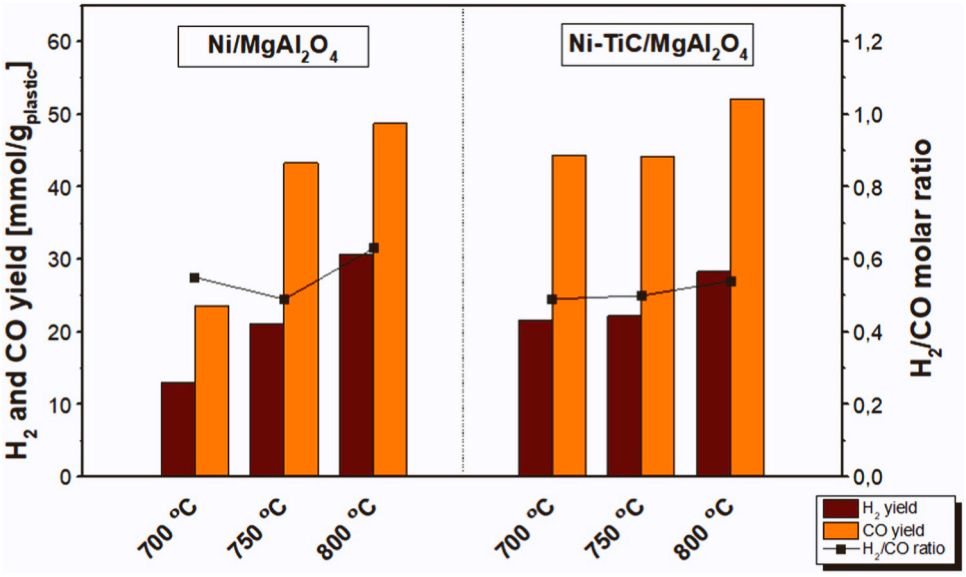

Fig. 14. Syngas (H_2 and CO) yield and composition in the pyrolysis combined with dry reforming of LDPE at different reforming temperatures.

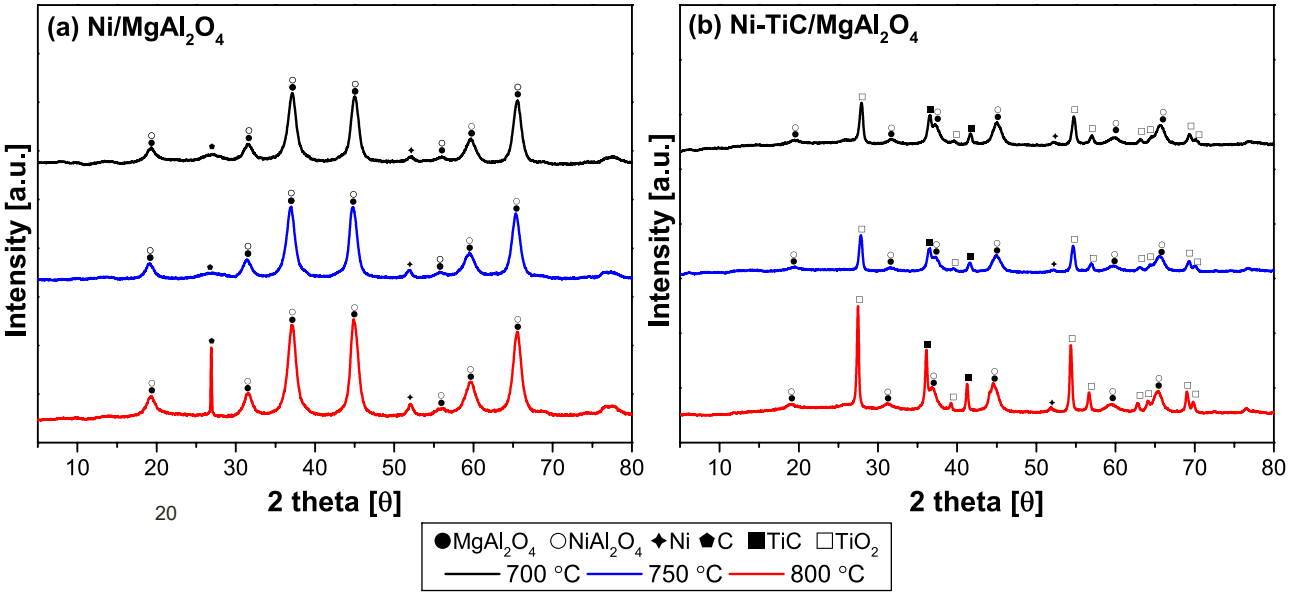

Fig. 15. XRD patterns of catalysts used at different reforming temperatures (700 °C, 750°C, 800 °C): a) $Ni/MgAl_2O_4$; (b) $Ni\text{-}TiC/MgAl_2O_4$.

exposure to air after the synthesis step, as well as oxidation with water molecules during the synthesis step [53,55,56]. In the case of nickel $Ni2p_{3/2}$ region the signal was deconvoluted into five component peaks at 862.5 eV, 857.4 eV, 855.8 eV and 853.1 eV indicating the presence of Ni^{2+}. The broad peak at binding energy centered at 862.5 eV was assigned to the Ni^{2+} shake-up satellite indicating the presence of NiO species [57].

Fig. 12 shows the BF-TEM images of the $Ni\text{-}TiC/MgAl_2O_4$ catalyst. In the images Fig. 12a, a phase with small spherical grains and larger particles up to 100 nm in size with a lamellar structure deposited on them can be distinguished. Both structures were characterized by the presence of embedded particles with sizes up to 10 nm, characterized by a higher contrast (darker spots in the images). To identify the individual phases, mapping and FFT (Fast Fourier Transform) analyses were performed. Magnesium-aluminum spinel crystallites (Fig. 12b), and titanium carbide crystallites (Fig. 12c) were observed, confirming the results of XRD analysis. The FFT analysis also showed the presence of nickel particles with size of 5–10 nm. Ni(200) and Ni(111) nickel crystallites deposited on $MgAl_2O_4$ and titanium carbide, respectively, were observed. To identify the distribution of phases present in the catalyst, a larger area of the catalyst was mapped. Maps of the individual elements are shown in Fig. 13. The map for magnesium closely corresponds with the map for aluminum, confirming the formation of $MgAl_2O_4$. At the same time, the map for titanium corresponds to the distribution of the carbon signal, indicating the presence of a titanium carbon fraction. EDS maps of the signals for individual elements confirmed the deposition of titanium carbide particles on the $MgAl_2O_4$ spinel and the distribution of nickel particles on both the spinel and carbide phases. Aggregates of nickel particles with sizes of up to 100 nm were also observed.

3.3. *Effect of reforming temperature*

$Ni\text{-}TiC/MgAl_2O_4$, as the most promising catalyst, was selected for further research to investigate the possibility of lowering the dry

MOST WIEDZY Downloaded from mostwiedzy.pl

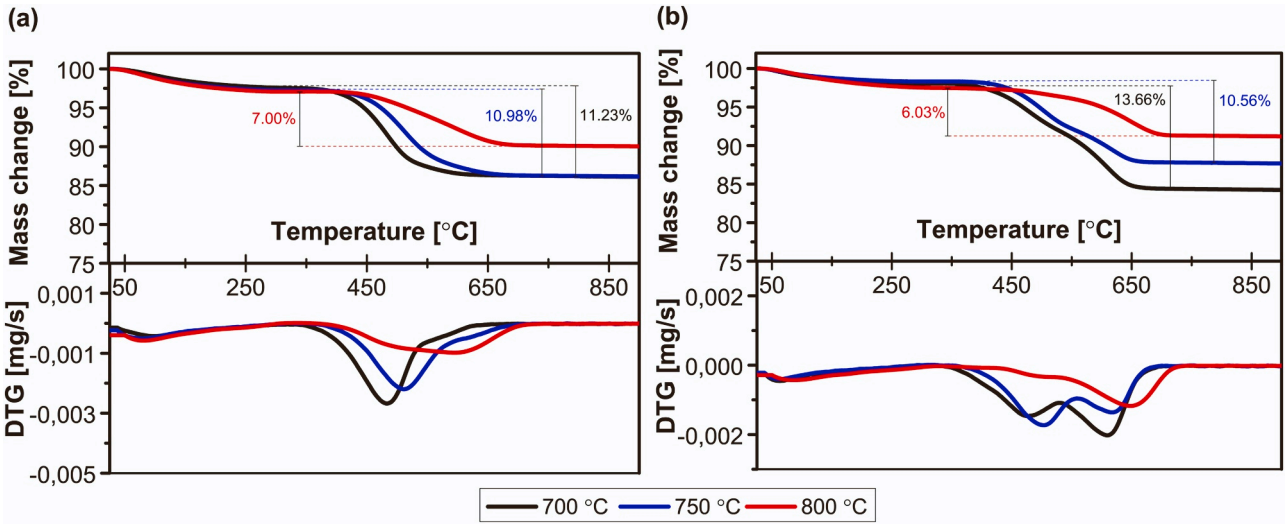

Fig. 16. TG and DTG curves of catalysts used at different reforming temperatures (700 °C, 750°C, 800 °C): a) $Ni/MgAl_2O_4$; (b) $Ni\text{-}TiC/MgAl_2O_4$.

Table 6
Effect of process pressure on product yields, H_2:CO molar ratio and CO_2 conversion in the pyrolysis combined with dry reforming of LDPE carried out over $NiMgAl_2O_4$ catalyst in 750 °C.

Pressure	Atm	2.5 bar
Syngas yield [mmol/$g_{plastic}$]	64.45	68.91
H_2 yield [mmol/$g_{plastic}$]	21.14	20.88
CO yield [mmol/$g_{plastic}$]	43.31	48.04
CH_4 yield [mmol/$g_{plastic}$]	5.10	4.80
H_2:CO molar ratio	0.49	0.43
CO_2 conversion [g/$g_{plastic}$]	2.92	2.57

Table 7
Effect of process pressure on product yields, H_2:CO molar ratio and CO_2 conversion in the pyrolysis combined with dry reforming of LDPE carried out over $Ni\text{-}TiC/MgAl_2O_4$ catalyst in 750 °C.

Pressure	Atm	2.5 bar
Syngas yield [mmol/$g_{plastic}$]	66.44	67.46
H_2 yield [mmol/$g_{plastic}$]	22.24	21.51
CO yield [mmol/$g_{plastic}$]	44.20	45.95
CH_4 yield [mmol/$g_{plastic}$]	2.77	5.08
H_2:CO molar ratio	0.50	0.47
CO_2 conversion [g/$g_{plastic}$]	2.82	2.84

reforming reaction temperature without significant reduction of the efficiency of syngas production. The catalyst was chosen due to the increased efficiency of syngas production in 800 °C compared to a conventional catalyst, while reducing the formation of carbon deposits that could lead to catalyst deactivation. In this aim, PCDR of LDPE experiments were carried out using reforming temperatures of 700 and 750 °C. Moreover, to further investigate the effect of modification of the catalyst with titanium carbide, analogous experiments were also carried out for the unmodified $NiMgAl_2O_4$ catalyst.

The product yields, CO_2 conversion, and synthesis gas H_2:CO molar ratios obtained in PCDR using different reforming temperatures are listed in Tables 4 and 5 for the $Ni/MgAl_2O_4$ and $Ni\text{-}TiC/MgAl_2O_4$ catalyst, respectively. The H_2 yield, CO yield, and H_2/CO molar ratio are presented in Fig. 14. It was demonstrated that regardless of the catalyst used, the efficiency of syngas production decreases with decreasing temperature. However, within the same temperatures, the syngas yields obtained for the catalyst modified with titanium carbide were higher. Modification of the catalyst increased the production of syngas from 36.61 mmol/g to 65.92 mmol/g for the reforming temperature of 700 °C and from 64.45 mmol/g to 66.44 mmol/g for 750 °C. Moreover, hydrogen yield was also higher for $Ni\text{-}TiC/MgAl_2O_4$ at these temperature conditions. As shown in Figure 14, H_2:CO ratios of obtained syngas over both catalysts were lower when temperature was decreased. CO_2 conversion decreased as well for all experiments carried out in lower temperatures, besides PCDR over $NiMgAl_2O_4$ in 700 °C. In this case CO_2 conversion was the highest equal to 4.52 mmol/g. However, syngas, carbon monoxide as well as hydrogen yields were the lowest. It indicates that carbon dioxide took a part in other reactions, which not favoured H_2 and CO production.

Used catalysts were further investigated using XRD and TG methods to analyse the impact of the reforming temperature on their structure and possible carbon formation. It was observed that XRD patterns of used $NiMgAl_2O_4$ catalyst (see Fig. 15a) at 700 and 750 °C contain halo at $2\theta = 26.9°$ related to amorphous carbon. In contrast, when reforming temperature was 800 °C, reflection attributed to graphitic carbon (reference card CSD: data_120017 (COD)) occurred at $2\theta = 26.9°$. On the other hand, on the XRD patterns of used $Ni\text{-}TiC/MgAl_2O_4$ (see Fig. 15b) additional diffraction peaks ($2\theta = 27.5°$, 39.2°, 54.6°, 56.7°, 62.8°, 64.1°, 69.0°, 69.8°) attributed to TiO_2 rutile phase were observed, regardless the reforming temperature. The presence of carbon cannot be confirmed on the basis of the obtained diffraction pattern in this case, due to the corresponding reflections may overlap with those attributed to TiO_2.

TG and DTG curves of used catalyst are presented in Fig. 16(a-b). It was observed that weight loss attributed to oxidation of formed carbon increases as the reforming temperature decreases for both catalysts. It can be attributed to the inhibitory effect of elevated reaction temperatures on the exothermic reactions involving carbon generation (Eqs. 3–5) [58].

$$2CO = C + CO_2 \quad (3)$$

$$CO_2 + 2\,H_2 = C + 2\,H_2O \quad (4)$$

$$H_2 + CO = H_2O + C \quad (5)$$

Modification of $NiMgAl_2O_4$ with TiC resulted in the higher weight loss when used reforming temperature was 700 °C. On the other hand, when catalysts were used at higher temperatures, weight loss decreased for $Ni\text{-}TiC/MgAl_2O_4$ from 10.98% to 10.56% and from 7.00% to 6.03% in comparison to unmodified catalyst used at reforming temperature 750 °C and 800 °C respectively. In the case of $NiMgAl_2O_4$ catalyst, the highest rate of weight loss was observed at the temperature of 485 °C

MOST WIEDZY Downloaded from mostwiedzy.pl

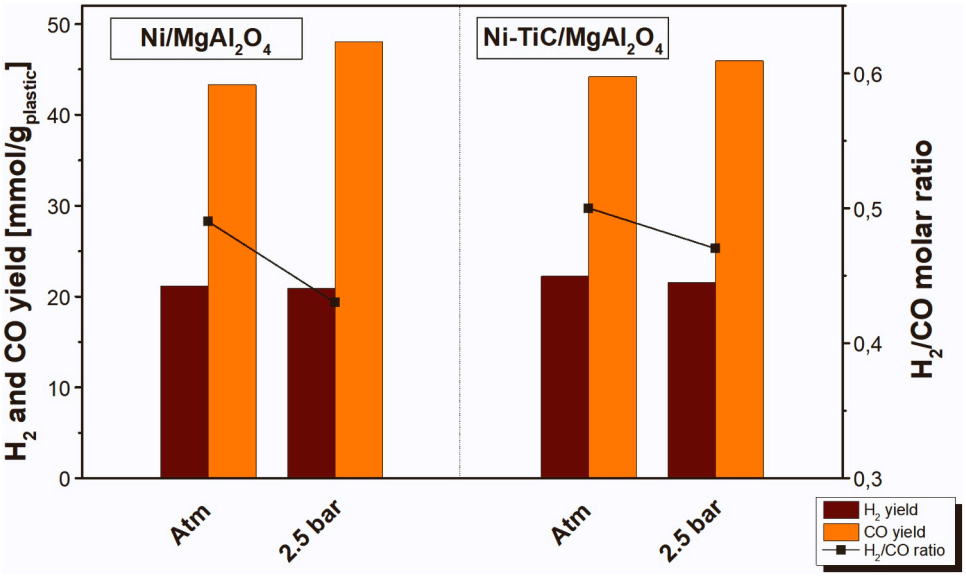

Fig. 17. Syngas (H_2 and CO) yield and composition in the pyrolysis combined with dry reforming of LDPE at different pressure conditions.

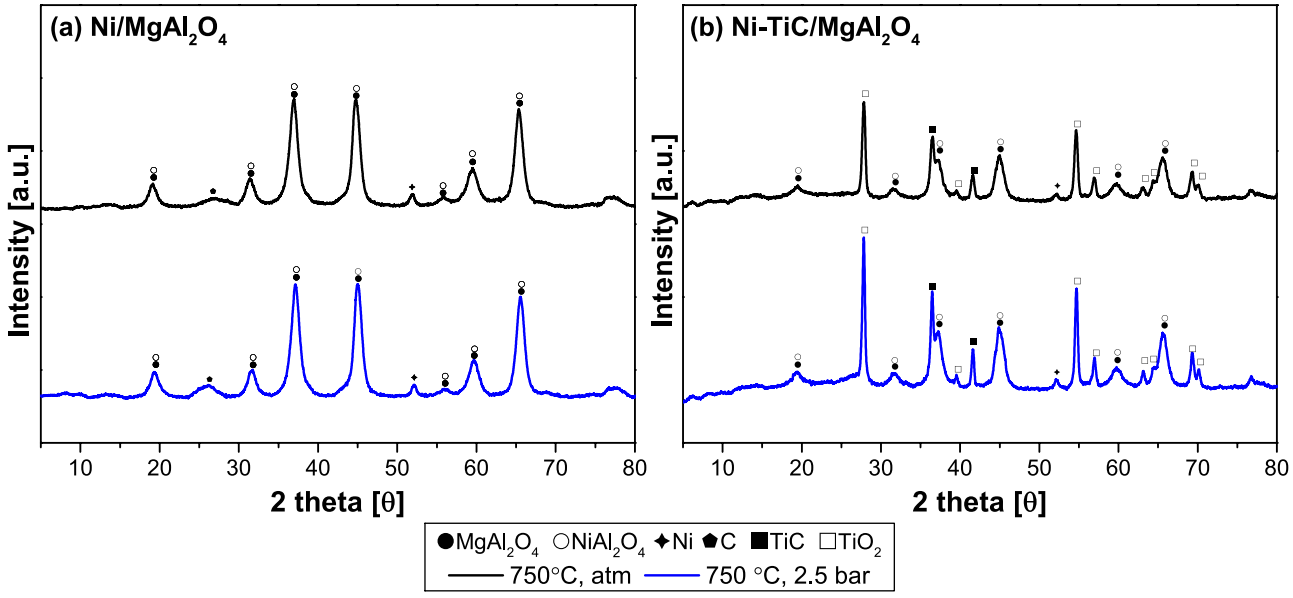

Fig. 18. XRD patterns of catalysts used at different pressure conditions: a) $Ni/MgAl_2O_4$; (b) $Ni\text{-}TiC/MgAl_2O_4$.

and 510 °C for catalyst used in 700 °C and 750 °C, respectively. It can be attributed to oxidation of amorphous carbon. In contrast, for catalyst used in 800 °C, weight loss was shifted to higher temperatures with the maximum rate at 600 °C, which can be related to formation of graphitic carbon. It is in line with the results of XRD analysis described above. For catalyst modified with TiC, two regions of weight loss were observed from 350 °C with maximum at 475 °C and 610 °C for catalyst used at reforming temperature of 700 °C. When reforming temperature was increased to 750 °C, maximums were shifted to 500 °C and 620 °C respectively. Weight loss at lower temperatures can be related to amorphous carbon, while region in higher temperatures is associated with oxidation of graphitic type carbon. In the case when $Ni\text{-}TiC/MgAl_2O_4$ catalyst was used at 800 °C, the weight loss is more pronounced at higher temperatures with a maximum loss rate at 650 °C, indicating the presence of higher amount of graphitic carbon.

3.4. *Effect of process pressure*

To investigate the effect of increased pressure conditions on PCDR process, additional tests were carried out at 2.5 bar over $Ni/MgAl_2O_4$ and $Ni\text{-}TiC/MgAl_2O_4$ catalysts with LDPE as a feedstock. The reforming temperature of 750 °C was selected to examine the possibility of increasing the syngas yields to values similar to those obtained at 800 °C with reduced energy cost. The product yields and syngas H_2:CO molar ratios obtained in PCDR of LDPE at different pressure conditions are given in Table 6 for the $NiMgAl_2O_4$ and Table 7 for $Ni\text{-}TiC/MgAl_2O_4$. It was revealed that increased process pressure resulted in increased syngas yields (from 64.45 to 68.91 mmol/g and 66.44–67.46 mmol/g for $NiMgAl_2O_4$ and $Ni\text{-}TiC/MgAl_2O_4$ respectively). However, H_2:CO molar ratios of obtained syngas decreased and the increased yield of syngas resulted from the increased efficiency of CO production (see Fig. 17). Comparing tested catalysts, it was demonstrated that modification of $NiMgAl_2O_4$ with TiC resulted in increased hydrogen yield as well as

MOST WIEDZY Downloaded from mostwiedzy.pl

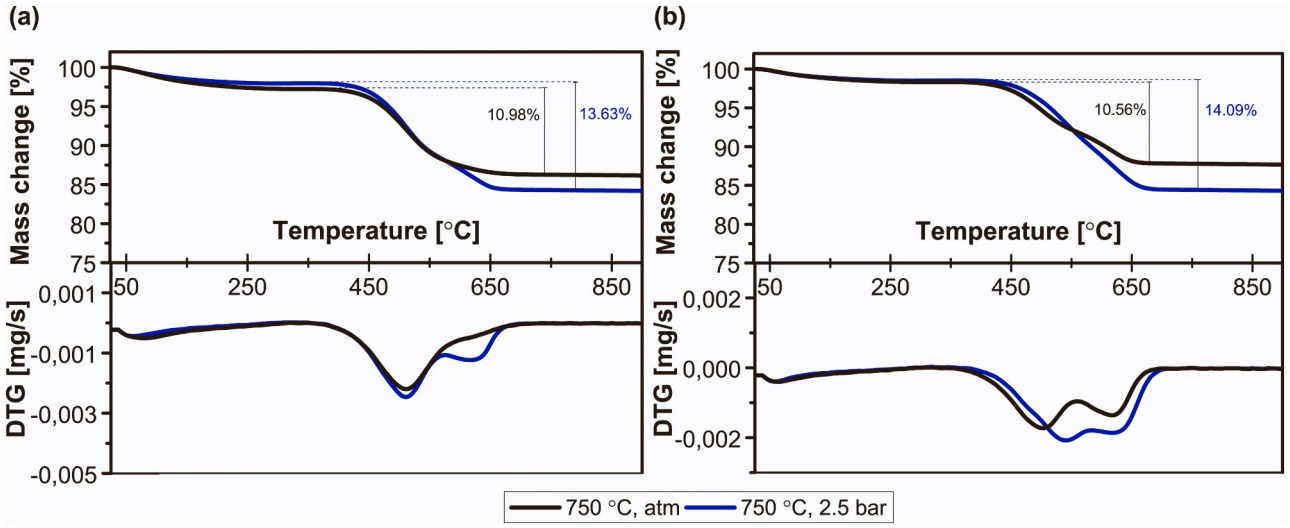

Fig. 19. TG and DTG curves of catalysts used at different pressure conditions: a) Ni/$MgAl_2O_4$; (b) Ni-TiC/$MgAl_2O_4$.

syngas H_2:CO molar ratio obtained under 2.5 bar conditions.

XRD patterns of the reacted catalysts are presented in Fig. 18. No additional diffraction peaks were observed for both catalysts used under 2.5 bar in comparison to atmospheric pressure conditions. According to the results of TG analysis (see Fig. 19), increased process pressure increases carbon formation. Weight loss attributed to oxidation of deposited carbon increased from 10.98% to 13.63% for PCDR over $NiMgAl_2O_4$ catalyst and from 10.56% to 14.09% for PCDR over Ni-TiC/$MgAl_2O_4$. Similar effect of increased pressure on formation of carbon deposits was observed by Shamsi et al. [59] who carried out dry reforming of methane under pressure of 1 bar and 14 bar. They observed that at condition of 1 bar main source of carbon was CO_2, while at elevated pressure carbon was generated both from CO_2 and CH_4. It may indicate that during PCDR of plastics, increased pressure may favour formation of carbon in dry reforming of pyrolysis-derived hydrocarbons. In addition, process pressure affected also the type of generated carbon. The increased rate of weight loss observed in DTG curves for the temperature in the range of 590 °C – 670 °C indicates that formation of graphite-type carbon is favoured under higher pressure conditions.

4. Conclusions

Metal carbide-modified nickel catalysts were synthesized and examined in pyrolysis combined with dry reforming of plastics (LDPE and PS). It was found that TiC, Mo_2C and WC affected BET surface area, reducibility and basicity of catalysts, and thus their catalytic activity and stability in PCDR process. Modification of catalysts with TiC and WC carbide allowed to successfully increase syngas yield in PCDR of LDPE, whereas modification of with TiC and Mo_2C in the PCDR of PS. Among the examined catalysts, Ni-TiC/$MgAl_2O_4$ catalyst showed highest efficiency in syngas production at reforming temperature of 800 °C as well as decreased carbon deposition regardless of the raw material used. Moreover, in all additional experiments involving different temperature (700 – 800 °C) and pressure (2.5 bar) conditions, the catalyst exhibited a higher synthesis gas yield compared to the conventional catalyst. Therefore, it was successful attempt of hindering catalyst deactivation caused by formation of carbon deposits and at the same time increasing effectivity of catalyst.

Furthermore, it was found that application of different metal carbide modified catalyst enables manipulation of synthesis gas composition, which is of great importance since different industrial processes require its different composition. It should be noted, that the same modified catalyst applied in PCDR of various feedstock may have different impact on H_2/CO molar ratio. For instance, modification of catalyst with WC resulted in decreased H_2/CO ratio in PCDR of LDPE, while in PCDR of PS catalyst showed increased H_2 content. Moreover, different TMC-modified catalysts lead to different product distributions, which gives opportunity to recover variety of products, depending on needs. Therefore, it can be concluded that application of specified catalyst depends on feedstock and required product composition.

It was demonstrated that elevated pressure and reforming temperature increased syngas yields, but had opposite influence on carbon formation – higher temperature decreased it, while elevated pressure resulted in increased carbon deposition. Moreover, It was indicated that increased temperature and pressure contribute to form graphitic-type carbon, instead of more unstable amorphous carbon.

Since metal carbides have not been investigated in the PCDR of waste plastics so far, the presented results are a significant contribution to the area. It was revealed that metal carbide based catalysts may be a promising alternative to conventional nickel catalysts. Results showed in the work constitute an important clue and set the direction for further research on PCDR of waste plastics. We believe that our work will contribute to further optimization of PCDR technology and its implementation in industrial scale in the future, allowing to successful realization of the concept of the circular economy and sustainable development.

Funding

The financial support for this study from Gdańsk University of Technology by the DEC-23/2020/IDUB/I.3.3 grant under the ARGENTUM—"Excellence Initiative—Research University" program is gratefully acknowledged.

CRediT authorship contribution statement

Ewelina Pawelczyk: Writing – original draft, Investigation, Conceptualization, Methodology, Visualization. **Izabela Wysocka**: Writing – review & editing, Conceptualization, Methodology, Funding acquisition, Project administration. **Tomasz Dymerski**: Investigation. **Jacek Gębicki**: Supervision, Resources.

Declaration of Competing Interest

The authors declare that they have no known competing financial interests or personal relationships that could have appeared to influence the work reported in this paper.

MOST WIEDZY Downloaded from mostwiedzy.pl

Data Availability

Data will be made available on request.

Appendix A. Supporting information

Supplementary data associated with this article can be found in the online version at doi:10.1016/j.cattod.2023.114414.

References

[1] Plastics Europe, Plastics—The Facts 2021; Plastics Europe: Brussels, Belgium, 2021
[2] R. Geyer, J.R. Jambeck, K.L. Law, Production, use, and fate of all plastics ever made, Sci. Adv. 3 (2017) 19–24, https://doi.org/10.1126/sciadv.1700782.
[3] S.M. Al-Salem, P. Lettieri, J. Baeyens, Recycling and recovery routes of plastic solid waste (PSW): a review, Waste Manag. 29 (2009) 2625–2643, https://doi.org/10.1016/j.wasman.2009.06.004.
[4] S.D. Anuar Sharuddin, F. Abnisa, W.M.A. Wan Daud, M.K. Aroua, A review on pyrolysis of plastic wastes, Energy Convers. Manag 115 (2016) 308–326, https://doi.org/10.1016/j.enconman.2016.02.037.
[5] European Parliament and the Council of the European Union, Official Journal of the European Union L 150: Legislation, Official Journal of the European Union. 2018 (2018) 26–42.
[6] K.O. Yoro, M.O. Daramola, CO_2 Emission Sources, Greenhouse Gases, and the Global Warming Effect, Elsevier Inc, 2020, https://doi.org/10.1016/b978-0-12-819657-1.00001-3.
[7] W.F. Lamb, T. Wiedmann, J. Pongratz, R. Andrew, M. Crippa, J.G.J. Olivier, D. Wiedenhofer, G. Mattioli, A.Al Khourdajie, J. House, S. Pachauri, M. Figueroa, Y. Saheb, R. Slade, K. Hubacek, L. Sun, S.K. Ribeiro, S. Khennas, S. De La Rue Du Can, L. Chapungu, S.J. Davis, I. Bashmakov, H. Dai, S. Dhakal, X. Tan, Y. Geng, B. Gu, J. Minx, A review of trends and drivers of greenhouse gas emissions by sector from 1990 to 2018, Environ. Res. Lett. 16 (2021), https://doi.org/10.1088/1748-9326/abee4e.
[8] E. Moe, J.K. S. Røttereng, The post-carbon society: rethinking the international governance of negative emissions, Energy Res. Soc. Sci. 44 (2018) 199–208, https://doi.org/10.1016/j.erss.2018.04.031.
[9] E. Pawelczyk, I. Wysocka, J. Gębicki, Pyrolysis Combined with the Dry Reforming of Waste Plastics as a Potential Method for Resource Recovery — A Review of, Catalysts. 12 (2022) 362.
[10] J.M. Saad, P.T. Williams, Pyrolysis-catalytic dry (CO_2) reforming of waste plastics for syngas production: influence of process parameters, Fuel 193 (2017) 7–14, https://doi.org/10.1016/j.fuel.2016.12.014.
[11] J.M. Saad, P.T. Williams, Catalytic dry reforming of waste plastics from different waste treatment plants for production of synthesis gases, Waste Manag. 58 (2016) 214–220, https://doi.org/10.1016/j.wasman.2016.09.011.
[12] B. Yan, X. Yang, S. Yao, J. Wan, M.N.Z. Myint, E. Gomez, Z. Xie, S. Kattel, W. Xu, J. G. Chen, Dry reforming of ethane and butane with CO_2 over PtNi/CeO2 bimetallic catalysts, ACS Catal. 6 (2016) 7283–7292, https://doi.org/10.1021/acscatal.6b02176.
[13] M.M. Sullivan, A. Bhan, Effects of oxygen coverage on rates and selectivity of propane-CO_2 reactions on molybdenum carbide, J. Catal. 357 (2018) 195–205, https://doi.org/10.1016/j.jcat.2017.11.004.
[14] A. Ochoa, J. Bilbao, A.G. Gayubo, P. Castaño, Coke formation and deactivation during catalytic reforming of biomass and waste pyrolysis products: a review, Renew. Sustain. Energy Rev. 119 (2020), https://doi.org/10.1016/j.rser.2019.109600.
[15] J.M. Saad, M.A. Nahil, C. Wu, P.T. Williams, Influence of nickel-based catalysts on syngas production from carbon dioxide reforming of waste high density polyethylene, Fuel Process. Technol. 138 (2015) 156–163, https://doi.org/10.1016/j.fuproc.2015.05.020.
[16] N. Czaplicka, A. Rogala, I. Wysocka, Metal (Mo, W, Ti) carbide catalysts: synthesis and application as alternative catalysts for dry reforming of hydrocarbons—a review, Int. J. Mol. Sci. 22 (2021), https://doi.org/10.3390/ijms222212337.
[17] C.E. Chan-Thaw, A. Villa, Metal carbides for biomass valorization, Appl. Sci. 8 (2018) 1–19, https://doi.org/10.3390/app8020259.
[18] Y. Ma, G. Guan, X. Hao, J. Cao, A. Abudula, Molybdenum carbide as alternative catalyst for hydrogen production – a review, Renew. Sustain. Energy Rev. 75 (2017) 1101–1129, https://doi.org/10.1016/j.rser.2016.11.092.
[19] C.G. Silva, F.B. Passos, V.T. da Silva, Influence of the support on the activity of a supported nickel-promoted molybdenum carbide catalyst for dry reforming of methane, J. Catal. 375 (2019) 507–518, https://doi.org/10.1016/j.jcat.2019.05.024.
[20] M.D. Porosoff, M.N.Z. Myint, S. Kattel, Z. Xie, E. Gomez, P. Liu, J.G. Chen, Identifying different types of catalysts for CO_2 reduction by ethane through dry reforming and oxidative dehydrogenation, Angew. Chem. Int. Ed. 54 (2015) 15501–15505, https://doi.org/10.1002/anie.201508128.
[21] F. Solymosi, R. Németh, A. Oszkó, The oxidative dehydrogenation of propane with CO_2 over supported Mo2C catalyst, Stud. Surf. Sci. Catal. 136 (2001) 339–344, https://doi.org/10.1016/s0167-2991(01)80326-8.
[22] M. Ronda-Lloret, V.S. Marakatti, W.G. Sloof, J.J. Delgado, A. Sepúlveda-Escribano, E.V. Ramos-Fernandez, G. Rothenberg, N.R. Shiju, Butane dry reforming catalyzed by cobalt oxide supported on Ti2AlC MAX phase, ChemSusChem 13 (2020) 6401–6408, https://doi.org/10.1002/cssc.202001633.
[23] T. Xiao, H. Wang, A.P.E. York, V.C. Williams, M.L.H. Green, Preparation of nickel-tungsten bimetallic carbide catalysts, J. Catal. 209 (2002) 318–330, https://doi.org/10.1006/jcat.2002.3651.
[24] Z. Yao, J. Jiang, Y. Zhao, F. Luan, J. Zhu, Y. Shi, H. Gao, H. Wang, Insights into the deactivation mechanism of metal carbide catalysts for dry reforming of methane via comparison of nickel-modified molybdenum and tungsten carbides, RSC Adv. 6 (2016) 19944–19951, https://doi.org/10.1039/c5ra24815a.
[25] Q. Zhang, L. Pastor-Pérez, S. Gu, T.R. Reina, Transition metal carbides (TMCS) catalysts for gas phase CO_2 upgrading reactions: a comprehensive overview, Catalysts 10 (2020), https://doi.org/10.3390/catal10090955.
[26] R.D. Barbosa, M.A.S. Baldanza, N.S. de Resende, F.B. Passos, V.L. dos S.T. da Silva, Nickel–promoted molybdenum or tungsten carbides as catalysts in dry reforming of methane: effects of variation in CH4/CO_2 molar ratio, Catal. Lett. 151 (2021) 1578–1591, https://doi.org/10.1007/s10562-020-03420-8.
[27] L. Zhang, Y. Yang, Z. Yao, S. Yan, X. Kang, Finding of a new cycle route in Ni/Mo2C catalyzed CH4-CO2reforming, Catal. Sci. Technol. 11 (2021) 479–483, https://doi.org/10.1039/d0cy02428g.
[28] S. Zhang, C. Shi, B. Chen, Y. Zhang, Y. Zhu, J. Qiu, C. Au, Catalytic role of β-Mo2C in DRM catalysts that contain Ni and Mo, Catal. Today 258 (2015) 676–683, https://doi.org/10.1016/j.cattod.2015.01.014.
[29] J.M. Encinar, J.F. González, Pyrolysis of synthetic polymers and plastic wastes. Kinetic study, Fuel Process. Technol. 89 (2008) 678–686, https://doi.org/10.1016/j.fuproc.2007.12.011.
[30] J.M. Saad, P.T. Williams, Pyrolysis-catalytic-dry reforming of waste plastics and mixed waste plastics for syngas production, Energy Fuels 30 (2016) 3198–3204, https://doi.org/10.1021/acs.energyfuels.5b02508.
[31] A.G. Buekens, H. Huang, Catalytic plastics cracking for recovery of gasoline-range hydrocarbons from municipal plastic wastes, 1998.
[32] I. Wysocka, N. Czaplicka, E. Pawelczyk, J. Karczewski, J. Sobczak, Z. Bielan, M. Maciejewski, B. Kościelska, A. Rogala, Novel sugar-based nickel-tungsten carbide catalysts for dry reforming of hydrocarbons, J. Ind. Eng. Chem. 124 (2023) 431–446, https://doi.org/10.1016/j.jiec.2023.04.038.
[33] K.B. Park, Y.S. Jeong, B. Guzelciftci, J.S. Kim, Two-stage pyrolysis of polystyrene: Pyrolysis oil as a source of fuels or benzene, toluene, ethylbenzene, and xylenes, Appl. Energy 259 (2020), 114240, https://doi.org/10.1016/j.apenergy.2019.114240.
[34] N. Cai, X. Li, S. Xia, L. Sun, J. Hu, P. Bartocci, F. Fantozzi, P.T. Williams, H. Yang, H. Chen, Pyrolysis-catalysis of different waste plastics over Fe/Al2O3 catalyst: high-value hydrogen, liquid fuels, carbon nanotubes and possible reaction mechanisms, Energy Convers. Manag 229 (2021), 113794, https://doi.org/10.1016/j.enconman.2020.113794.
[35] R. Jalali, B. Nematollahi, M. Rezaei, M. Baghalha, Mesoporous nanostructured Ni/MgAl2O4 catalysts: Highly active and stable catalysts for syngas production in combined dry reforming and partial oxidation, Int J. Hydrog. Energy 44 (2019) 10427–10442, https://doi.org/10.1016/j.ijhydene.2018.12.186.
[36] N. Hadian, M. Rezaei, Z. Mosayebi, F. Meshkani, CO 2 reforming of methane over nickel catalysts supported on nanocrystalline MgAl 2O 4 with high surface area, J. Nat. Gas. Chem. 21 (2012) 200–206, https://doi.org/10.1016/S1003-9953(11)60355-1.
[37] M. Zarei, F. Meshkani, M. Rezaei, Preparation of mesoporous nanocrystalline Ni-MgAl2O4 catalysts by sol-gel combustion method and its applications in dry reforming reaction, Adv. Powder Technol. 27 (2016) 1963–1970, https://doi.org/10.1016/j.apt.2016.06.028.
[38] N. Zhang, Z. Yang, Z. Chen, Y. Li, Y. Liao, Y. Li, M. Gong, Y. Chen, Synthesis of sulfur-resistant TiO2-CeO2 composite and its catalytic performance in the oxidation of a soluble organic fraction from diesel exhaust, Catalysts 8 (2018), https://doi.org/10.3390/catal8060246.
[39] V.G. Deshmane, S.L. Owen, R.Y. Abrokwah, D. Kuila, Mesoporous nanocrystalline TiO2 supported metal (Cu, Co, Ni, Pd, Zn, and Sn) catalysts: effect of metal-support interactions on steam reforming of methanol, J. Mol. Catal. A Chem. 408 (2015) 202–213, https://doi.org/10.1016/j.molcata.2015.07.023.
[40] N.R. Shiju , Science &, 8 (2018).
41] J.Guan, C. Xu, Z. Wang, Y. Yang, B. Liu, F. Shang, Y. Shao, Q. Kan, Selectiveoxidation of isobutane and isobutene to methacrolein over Te-Mo mixed oxidecatalysts, Catal Letters. 124 (2008) 428–433.https://doi.org/10.1007/s10562-008-9496-3.
[42] A. Samsuri, F. Salleh, T.S.T. Saharuddin, R. Othaman, MohdA. Yarmo, Study on the reduction behaviour of nickel doped molybdenum trioxide by using carbon monoxide as reductant, Int. J. Chem. Eng. Appl. 7 (2016) 16–21, https://doi.org/10.7763/ijcea.2016.v7.534.
[43] J. Harmel, T. Roberts, Z. Zhang, G. Sunley, P. de Jongh, K.P. de Jong, Bifunctional molybdenum oxide/acid catalysts for hydroisomerization of n-heptane, J. Catal. 390 (2020) 161–169, https://doi.org/10.1016/j.jcat.2020.08.004.
[44] F. Salleh, engku S.T. Saharuddin, A. Samsuri, R. Othaman, MohdA. Yarmo, Effect of zirconia and nickel doping on the reduction behavior of tungsten oxide in carbon monoxide atmosphere, Int. J. Chem. Eng. Appl. 6 (2015) 389–394, https://doi.org/10.7763/ijcea.2015.v6.516.
[45] K.B. Ghoreishi, M.A. Yarmo, N.M. Nordin, M.W. Samsudin, Enhanced catalyst activity of WO3 using polypyrrole as support for acidic esterification of glycerol with acetic acid, J. Chem. (2013), https://doi.org/10.1155/2013/264832.
[46] J. Ten Dam, D. Badloe, A. Ramanathan, K. Djanashvili, F. Kapteijn, U. Hanefeld, Synthesis, characterisation and catalytic performance of a mesoporous tungsten silicate: W-TUD-1, Appl. Catal. A Gen. 468 (2013) 150–159, https://doi.org/10.1016/j.apcata.2013.08.025.
[47] M. Thommes, K. Kaneko, A.V. Neimark, J.P. Olivier, F. Rodriguez-Reinoso, J. Rouquerol, K.S.W. Sing, Physisorption of gases, with special reference to the

MOST WIEDZY Downloaded from mostwiedzy.pl

evaluation of surface area and pore size distribution (IUPAC Technical Report), Pure Appl. Chem. 87 (2015) 1051–1069, https://doi.org/10.1515/pac-2014-1117.
[48] M.D. Donohue, G.L. Aranovich, Classification of Gibbs adsorption isotherms, Adv. Colloid Interface Sci. 76–77 (1998) 137–152, https://doi.org/10.1016/S0001-8686(98)00044-X.
[49] I. Wysocka, A. Mielewczyk-Gryń, M. Łapiński, B. Cieślik, A. Rogala, Effect of small quantities of potassium promoter and steam on the catalytic properties of nickel catalysts in dry/combined methane reforming, Int J. Hydrog. Energy 46 (2021) 3847–3864, https://doi.org/10.1016/j.ijhydene.2020.10.189.
[50] A.S. Rajan, S. Sampath, A.K. Shukla, An in situ carbon-grafted alkaline iron electrode for iron-based accumulators, Energy Environ. Sci. 7 (2014) 1110–1116, https://doi.org/10.1039/c3ee42783h.
[51] S. López-Romero, J. Chávez-Ramírez, Synthesis of TiC thin films by CVD from toluene and titanium tetrachloride with nickel as catalyst, Matér. Rio De. Jan. 12 (2007) 487–493, https://doi.org/10.1590/s1517-70762007000300009.
[52] X.Y. Liu, M. Huang, H.L. Ma, Z.Q. Zhang, J.M. Gao, Y.L. Zhu, X.J. Han, X.Y. Guo, Preparation of a carbon-based solid acid catalyst by sulfonating activated carbon in a chemical reduction process, Molecules 15 (2010) 7188–7196, https://doi.org/10.3390/molecules15107188.
[53] A. Ignaszak, C. Song, W. Zhu, J. Zhang, A. Bauer, R. Baker, V. Neburchilov, S. Ye, S. Campbell, Titanium carbide and its core-shelled derivative TiC@TiO 2 as catalyst supports for proton exchange membrane fuel cells, Electro Acta 69 (2012) 397–405, https://doi.org/10.1016/j.electacta.2012.03.039.
[54] C. Wang, S. Zhang, M. Zheng, R. Shu, S. Gu, J. Guo, C. Liu, J. Tang, J. Chen, X. Wang, Atomically thin titanium carbide used as high-efficient, low-cost and stable catalyst for oxygen reduction reaction, Int J. Hydrog. Energy 45 (2020) 6994–7004, https://doi.org/10.1016/j.ijhydene.2019.12.195.
[55] A. Grzegórska, P. Głuchowski, J. Karczewski, J. Ryl, I. Wysocka, K. Siuzdak, G. Trykowski, K. Grochowska, A. Zielińska-Jurek, Enhanced photocatalytic activity of accordion-like layered Ti<inf>3</inf>C<inf>2</inf> (MXene) coupled with Fe-modified decahedral anatase particles exposing {1 0 1} and {0 0 1} facets, Chem. Eng. J. 426 (2021), https://doi.org/10.1016/j.cej.2021.130801.
[56] I. Wysocka, J. Karczewski, A. Gołąbiewska, M. Łapiński, B.M. Cieślik, M. Maciejewski, B. Kościelska, A. Rogala, Nickel phase deposition on V2CTx/V2AlC as catalyst precursors for a dry methane reforming: The effect of the deposition method on the morphology and catalytic activity, Int J. Hydrog. Energy 48 (2023) 10922–10940, https://doi.org/10.1016/j.ijhydene.2022.12.109.
[57] A.M. Tarditi, N. Barroso, A.E. Galetti, L.A. Arrúa, L. Cornaglia, M.C. Abello, XPS study of the surface properties and Ni particle size determination of Ni-supported catalysts, Surf. Interface Anal. 46 (2014) 521–529, https://doi.org/10.1002/sia.5549.
[58] M.K. Nikoo, N.A.S. Amin, Thermodynamic analysis of carbon dioxide reforming of methane in view of solid carbon formation, Fuel Process. Technol. 92 (2011) 678–691, https://doi.org/10.1016/j.fuproc.2010.11.027.
[59] A. Shamsi, C.D. Johnson, Effect of pressure on the carbon deposition route in CO_2 reforming of 13CH4, : Catal. Today (2003) 17–25, https://doi.org/10.1016/S0920-5861(03)00296-7.

MOST WIEDZY Downloaded from mostwiedzy.pl